EXAMINING RUTHENIUM CHROMOPHORES FOR THE PHOTOCHEMICAL REDUCTION OF CO_2 TO METHANOL

by

DAVID J BOSTON

Presented to the Faculty of the Graduate School of
The University of Texas at Arlington in Partial Fulfillment
of the Requirements
for the Degree of

DOCTOR OF PHILOSOPHY

THE UNIVERSITY OF TEXAS AT ARLINGTON
December 2013

ACKNOWLEDGEMENTS

I would like to thank Dr. MacDonnell for the knowledge and support given to me over the course of my Ph.D. work. His guidance in both professional and person life have been a great help and will help me for years to come. The understanding he has displayed has helped me to grow and mature as a chemist and a person, I can only hope to pay it forward as I progress with my professional career.

To my family I want to say thank you for the support over the last few years as I have worked on this degree. I know it has been stressful for everyone as my life has been taken up with school and research. My son and daughter have been the joy in my life even when I am not able to spend the time with them that I would like. They have given me more love and happiness than I could ever hope to receive. My parents have been supportive of my decisions even when they have not fully agreed with them, for this I want to say thank you.

To my lab mates, thank you for your support all these years. You have helped me achieve something that I could not have done alone. The help you have given me with presentations and papers is immeasurable and appreciated more than I can express in words. Your friendship has given me strength to move forward with my life and continue through my darkest times. I hope for the best for all of you. I would like to especially thank Norma de Tacconi and Reynaldo O. Lezna for the help obtaining data in Chapter 3, especially the reflective spectroelecctrochemical data Reynaldo obtained for me. Without him this data would not have been possible. I greatly appreciate the lessons and guidance on electrochemistry and help that Norma provide over the years. The work she did getting data the formate and formaldehyde from the electrolysis is also greatly appreciated

August 29, 2013

ABSTRACT

EXAMINING RUTHENIUM CHROMOPHORES FOR THE

PHOTOCHEMICAL REDUCTION OF

CO_2 TO METHANOL

David J. Boston, PhD

The University of Texas at Arlington 29th, 2013

Supervising Professor: Frederick M. MacDonnell

Our consumption of energy for transportation and electricity has been growing as quickly as our population. As this demand for energy increases we increase our production of carbon dioxide by the burning of fossil fuels to try and meet this increasing demand. A sustainable method to convert carbon dioxide (CO_2) to a viable liquid fuel is one potential way in which both the increasing energy demand and increasing CO_2 concentration issues can both be helped. Currently such methods being investigated include thermal, electrochemical, and photochemical processes. Because thermal conversion is not an ideal situation because of the requirement of strong reducing agents or extreme conditions such as steam reformation reactions, we need to find better alternatives such as electrochemical and photochemical methods. Both electrochemical and photochemical methods have the ability to be sustainable, however, the vast majority of these systems are limited to producing CO and/or formic acid, with only a few performing deeper reduction to products such formaldehyde, methanol and methane. All of the systems capable of reducing CO_2 past two electrons involve either a heterogeneous catalyst (e.g. TiO_2) or an electrode.

In recent times Bocarsly and coworkers have shown that pyridine was capable of reducing CO_2 to methanol through a sequential process of proton and electron transfers. This process seems to start with the formation of a CO_2-pyridine adduct in solution that is reduced one more time to form formate/formic acid. The next reduction is a slow process and allows for a buildup of formate in solution leading to a higher formate concentration in solution. The subsequent reductions seem to occur very rapidly and form methanol at good efficiencies. Theoretical work done recently has argued for the necessity of the Pt, Pd, or GaP surface in the electrochemistry. Carter and coworkers have claimed that the surface of the electrode is a necessary part of the catalysis with the pyridinium being only a cocatalyst for the reduction of CO_2. However, Musgrave and coworkers predict that the homogeneous reductions can take place with the aid of water molecules in solution. They allow for a PCET process to take place between the CO_2 and the pyridinium radical. This would allow for a second pathway for the catalytic reduction of CO_2 to methanol.

Work done during this dissertation has shown that the photochemical reduction of carbon dioxide to methanol is possible using pyridine in a similar manner to Bocarsly and coworkers in their electrochemical system. By replacing the electrode with $Ru(phen)_3Cl_2$ it is still possible to drive the reaction using excited states of the chromophore to provide the electrons with enough energy to reduce the pyridinium to the radical species. This system has been shown to produce up to 66 μM methanol after 6 hours of irradiation of 470 nm light. Production of formate is also observed, with ~27 mM being observed within the first hour of irradiation.

This system was further investigated with the incorporation of the pyridine catalyst into a chromophore system using the complex $[Ru(phen)_2dppz](PF_6)_2$, $[Ru(phen)_2pbtp\alpha](PF_6)_2$, and $[Ru(phen)_2pbtp\beta](PF_6)_2$. Cyclic voltammetry experiments for these complexes show similar reduction potentials for with ~100 mV difference between

them with $[Ru(phen)_2dppz](PF_6)_2$ being the most negative and $[Ru(phen)_2pbtp\beta](PF_6)_2$ being the most positive. When the electrolyte solution was saturated with CO_2 only $[Ru(phen)_2pbtp\alpha](PF_6)_2$ and $[Ru(phen)_2pbtp\beta](PF_6)_2$ showed a response signifying catalysis was taking place. Initial photochemical tests with these complexes showed that $[Ru(phen)_2pbtp\alpha](PF_6)_2$ seemed to undergo dimer formation in the absence of CO_2 with $[Ru(phen)_2pbtp\beta](PF_6)_2$ forming a singly reduced species that is oxidized upon introduction of additional CO_2. Electrolysis of $[Ru(phen)_2pbtp\beta](PF_6)_2$ produces ~900 μM methanol with both CO and formate being produced as well. Photolysis of $[Ru(phen)_2pbtp\beta](PF_6)_2$ in DMF with 1 M H_2O and 0.1M TEA, no CO formation observed, however, both methanol and formic acid were observed after 1 hours of irradiation with methanol reaching 45 μM, 285 μM formaldehyde and 650 μM formate.

TABLE OF CONTENTS

LIST OF ILLUSTRATIONS

LIST OF TABLES

LIST OF ABREVIATIONS

tb-cabinol..... tris(4'-methyl-2,2'-bipyridyl-4-methyl)carbinol

dmb ..... 4,4’-dimethyl-2,2’-bipyridyl

TEA .....triethylamine

TEOA..... triethanolamine

BNAH 1-Benzyl-1,4-dihydronicotinamide

H_2A ..... Ascorbic Acid

bpz.....2,2'-bipyrazine

HMD 5,7,7,12,14,14-hexamethyl-1,4,8,11-tetraazacyclotetradeca-4,11-diene

cyclam 1,4,8,11-tetraazacyclotetradecane

pr-cyclam..... 6-((p-methoxybenzyl)pyridin-4-yl)methyl

..... -1,4,8,11 –tetraazacyclotetradecan

MV .....methyl viologen

phen 1,10-phenanthroline

bpy.....2,2’-bipyridine

EDTA.....ethylenediaminetetraacetate

TPA ..... tripropylamine

TMA..... trimethylamine

TPP 5,10,15,20-Tetraphenylporphin

TBtA .....tributylamine

TPtA .....tripentylamine

TiBA.....triisobutylamine

TMEDA..... N,N,N,N-tetramethylethylenediamine

{[Zn(TPP)]/[$Re(CO)_3$(pic)(bpy)]} .....5-[4-[(2-methoxy-4-([rhenium (I) tricarbonyl

.....(3-picoline)]4-methyl-2,2’-bipyridine-4’-carboxyamidyl)

.... carboxyamidyl) phenyl] phenyl]-10,15,20-triphenyl

..... porphyrinatozinc(II)

2-m-8-Hq 2-methyl-8-hydroxyquinoline

2-Qui..... 2-quinoxalinol, Hiq = Hydroxyisoquinoline

4-m-1,10-Phen 4-methyl-1,10-phenanthroline

salophen..... (4-acetamidophenyl) 2-hydroxybenzoate

dophen .....2,9-bis(2-hydroxyphenyl)-1,10-phenanthroline

tpy..... 2,2';6',2"-terpyridine

N-MeIm.....1-methyl-imidazole

tBu-bpy .....4,4'-tertbutyl-2,2'-bipyridine

dppm ..... 1,1-Bis(diphenylphosphino)methane

dppe ..... 1,1-Bis(diphenylphosphino)ethane

dmg ..... dimethylglyoxime

COD 1,5-Cyclooctadiene

tmdnTAA ..... 5,7,12,14-tetramethyldinaphtho[b,i][1,4,8,11]tetraaza[14]annulene

HACD 1,3,6,9,11,14-hexaazacyclohexadecane

decyclam 1,8-diethyl-1,3,6,8,10,13-hexaazacyclotetradecane

TBA ..... tetra-N-butylammonium

TEtA ..... tetra-N-ethylammonium

TMA..... tetra-N-methylammonium

CHAPTER 1

ELECTRO- AND PHOTOCATALYTIC REDUCTION OF CO_2

1.1 Introduction and Scope

The use of fossil fuels has powered our society since the industrial revolution, however we have yet to move past the burning of these fuels. Burning these fuels contributes to global climate change and buildup of carbon dioxide (CO_2) in our atmosphere. Scientists have looked at how to reduce the rate of CO_2 production and a number of alternative energy sources have been investigated, solar, wind, wave, nuclear, etc. However, transportation consumes 20% of our yearly global energy production and could benefit from a renewable fuel. By reducing CO_2 back to a fuel that could be utilized by the transportation sector it would help to solve two problems at one, alleviate the strain of energy production on the transportation sector and reduce the rate that we are increasing CO_2 concentrations in the atmosphere.

We can perform this reduction using electricity, light or strong chemical reductants. The last of these three is unsustainable due to the amount of energy input required to produce this strong reductants. However, the catalytic reduction of CO_2 to fuels and organic compounds using light, electricity, or a combination of both, is not a new topic. References to this topic date back to the 1800s,[3] although rapid progress was made only since the 1970s. As elaborated below, a major challenge relates to the fact that the CO_2 molecule is extremely stable and is kinetically inert. A number of review articles and book chapters already exist on what has been accomplished on this challenging R&D topic.[6-16] This chapter contains an overview of recent developments in molecular catalysts for CO_2 reduction, summarized in Table 1.2 and Table 1.3. The

focus here will be on the use of homogeneous inorganic molecules and organic molecules to catalyze the reduction of CO_2. Biochemical or bioelectrochemical approaches (for example, see Ref. 12), are clearly of interest and importance from a comparative perspective of the artificial photosynthesis approach, however, this will not be discussed below.

At this point it seems important to review the various terminologies as used in the literature to clarify to everyone what is being discussed. A *homogeneous* CO_2 reduction system consists of an assembly of dissolved (molecular) catalyst that may be present in addition to a light absorber, sacrificial electron donor, and/or electron relay all in the same solution. In some cases, the light absorbing function may be built into the same catalyst molecule but the key obviously is that all participating components are present in the same phase. A *heterogeneous* system, on the other hand, has the catalyst present in a different (i.e., solid) phase. This includes metal catalysts supported on inert material and colloidaly systems.

The term “photoelectrochemical” has been largely applied in the literature to situations involving a semiconductor electrode whereas in the present context, we apply this terminology to denote situations involving either the traditional semiconductor/liquid junctions or catalyst molecules that serve the dual functions of both light absorption and electron transfer mediation. Alternate descriptions based on “electrocatalytic” and “photocatalytic” systems are synonymous and denote approaches wherein the CO_2 reduction is driven electrochemically and with the assistance of light, respectively. On the other hand, *photochemical* systems are best reserved for approaches based on colloidal suspensions of metal or inorganic semiconductor nanoparticles or purely homogeneous systems with molecular catalysts in solution. .

This dissertation will focus on the use of homogeneous ruthenium complexes to drive the photochemical conversion carbon dioxide to methanol using a pyridinium and pyridinium type catalysts. Chapter 2 will discuss the intermolecular photosystem that incorporates Bocarsly's pyridinium catalyst with ruthenium polypyridyl will be discussed and along with current improvements on the system. Chapter 3 will talk about an intramolecular photochemical catalyst and its electrochemical properties. Both of these systems are novel because of the limited number of systems that go beyond a two electron reduction product for the reduction of carbon dioxide where these catalyst go to methanol, a six electron and six proton reduction product.

1.2 Thermodynamics of CO_2 Reduction

Equations 1-6 below show the various products resulting from the reduction of CO_2 ranging from a one-electron reduction to the radical anion all the way to an 8 e^- deep reduction to methane. Multiple proton-coupled electron transfer (PCET) steps occur in Equations 2-6 and herein lies the rich electrochemistry inherent with this system. Given that these electrochemical processes are pH-dependent, the potentials below are given at pH 7 in aqueous solution versus the normal hydrogen electrode (NHE), 25 °C, 1 atm gas pressure, and 1 M for the solutes.[7,17]

Table 1.1 The reduction potentials of various reduction reactions of CO_2

$CO_2 + e^- \rightarrow CO_2^{\bullet -}$	$E^\circ = -1.90$ V	(1)
$CO_2 + 2\ e^- + 2\ H^+ \rightarrow CO + H_2O$	$E^\circ = -0.53$ V	(2)
$CO_2 + 2\ e^- + 2\ H^+ \rightarrow HCOOH$	$E^\circ = -0.61$ V	(3)
$CO_2 + 4\ e^- + 4\ H^+ \rightarrow H_2CO + H_2O$	$E^\circ = -0.48$ V	(4)
$CO_2 + 6\ e^- + 6\ H^+ \rightarrow H_3COH + H_2O$	$E^\circ = -0.38$ V	(5)
$CO_2 + 8\ e^- + 8\ H^+ \rightarrow CH_4$	$E^\circ = -0.24$ V	(6)

While progress on the concerted $2e^-$ - $2H^+$ reduction to CO or formate has been impressive (see Table 1.2 and Table 1.3 and the information below), more useful products (fuels) such as methanol and methane necessitate multiple electron and proton transfers and the kinetic barriers associated with these are formidable as briefly discussed next.

1.3 Energetics of CO_2 Reduction

1.3.1 General Remarks

The terms “electrocatalytic“ and “photocatalytic” are used herein in a generic sense with the implicit and important recognition that Reactions 1-6 above are endergonic with ΔG values ranging from 1.90 eV to 8.31 eV respectively. Putting an electron into the linear and inert CO_2 molecule (Reaction 1) entails a steep energy cost because of the resultant structural distortion.[18] This is reflected in the very negative reduction potential for Reaction (1) above. Thus this radical formation step is very energy-inefficient and the steep activation barrier associated with it, must be avoided via the use of a catalyst.[19,20] From an electrochemical perspective, this translates to sizeable “overpotentials” (spanning several hundred mV) for driving this reduction process.[19,20] Thus a catalyst molecule, by interacting strongly with the radical anion, can reduce this energy barrier. This is the essence of many of the catalysis-based approaches to be discussed below.

Table 1.2 Photochemical systems for CO_2 reductions with reaction conditions, catalysts, chromophore, and products

	Chromophore	Cat/relay	Donor	Solvent	Product	Φ (mol/einsteins)	TON/ TOF	pH	Irr. time h	λ nm	Ref
1	$Ru(bpy)_3^{2+}$		TEOA	15%H_2O in DMF	$HCOO^-$	0.049	19/9.5				151
2	$Ru(bpy)_3^{2+}$		TEOA	15%H_2O in DMF	$HCOO^-$	0.096	43/21.5				151
3	$Ru(bpy)_3^{2+}$	MV^{2+}	TEOA. EDTA	H_2O	$HCOO^-$	0.01	75/18.8		4		152
4	$Ru(bpy)_3^{2+}$	Co^{2+}/bpy	TEA, TPA, TEOA, TMA	MeCN/donor/ H_2O , 3:1:1 (vol/vol)	CO, H_2		9/0.4		22		153
5	$Ru(bpy)_3^{2+}$	Co^{2+}/2,9-Me_2phen	TEA, TPA, TMA, TBA, TPtA, TiBA, TMEDA	MeCN or DMF/donor/ H_2O , 3:1:1 (vol/vol), DMF/ H_2O 3:2	CO, H_2	0.012 (CO), 0.065 (H_2)		8.6	26		154
6	$Ru(bpy)_3^{2+}$	$Ru(bpy)_2(CO)_2^{2+}$	TEOA	H_2O /DMF 1:9 and DMF	$HCOO^-$	2% , 1%		6/9.5	10		41, 42, 138
7	$Ru(bpy)_3^{2+}$	$Ru(bpy)_2(CO)_2^{2+}$	BNAH	H_2O /DMF 1:9	$HCOO^-$, CO	0.03 ($HCOO^-$), 0.15 (CO)	50, 125	6/9.5	10		41, 42, 138
8	$Ru(bpy)_3^{2+}$	$Ru(bpy)_2(CO)H^+$	TEOA		$HCOO^-$	0.15	161/80.5				151
9	$Ru(bpy)_3^{2+}$	$Ru(bpy)_2(CO)X^{n+}$ X=Cl,CO	TEOA		$HCOO^-$		163/81.5(X=Cl) 54/27 (X=CO)				151

Table 1.2 - Continued

	Chromophore	Cat/relay	Donor	Solvent	Product	Φ (mol/einsteins)	TON/ TOF	pH	Irr. time h	λ nm	Ref
10	$Ru(bpy)_3^{2+}$	$Co(HMD)^{2+}$	H_2A		CO, H_2						77
11	$Ru(bpy)_3^{2+}$	$Ni(cyclam)^{2+}$	H_2A	H_2O	CO, H_2	0.001 (CO)		4	22		76, 78
12	$Ru(bpy)_3^{2+}$	$Ni(Pr\text{-}cyclam)^{2+}$	H_2A	H_2O	CO, H_2		ca. 0.005 (CO)	5.1	4		79
13	$Ru(bpy)_3^{2+}$	Bipyridinium$^+$, Ru/OS Colloid	TEOA	H_2O	CH_4, H_2	10^{-4} (CH_4), 10^{-3}(H_2)		7.8	2		87
14	$Ru(phen)_3^{2+}$	$Ni(cyclam)^{2+}$	H_2A	H_2O	CO, H_2		< 0.1	4	22		78
15	$Ru(phen)_3^{2+}$	Pyridine	H_2A	H_2O	CH_3OH	7.22 x 10^-7	0.9	5	6	470	86
16	$Ru(bpz)_3^{2+}$	Ru colloid	TEOA	H_2O /EtOH 2:1	CH_4	0.04%	15	9.5	2		87, 88
17	$Ru(dmb)_3^{2+}$	$ReCl(dmb)(CO)_3$	BNAH	DMF:TEOA 5:1	CO	0.062	101/6.3		16	≥ 500	69
18	$[Ru(phen)_2(phenC_1cyclam)Ni]^{2+}$		H2A	H_2O	CO, H_2		< 0.1	5.1	4		79
19	$[(dmb)_2Ru(MebpyC_3OHMebpy)Re(CO)_3Cl]^{2+}$		BNAH	DMF:TEOA 5:1	CO	0.12	170/10.7		16	≥ 500	69
20	$[(dmb)_2Ru(MebpyC_nH_{2n}Mebpy)Re(CO)_3Cl]^{2+}$		BNAH	DMF:TEOA 5:1	CO	0.13 (n=2), 0.11 (n=4,6)	180/15 (n-2), 120/10 (n=4,6)		16	< 500	73

Table 1.2 - Continued

	Chromophore	Cat/relay	Donor	Solvent	Product	Φ (mol/einsteins)	TON/ TOF	pH	Irr. time h	λ nm	Ref
21	$[(dmb)_2Ru(MebpyC_3OHMebpy)Re(CO)_3\{P(POEt)_3\}]^{3+}$		BNAH		CO	0.21	232/19.3				70
22	$[Ru\{(MebpyC_3OHMebpy)Re(CO)_3Cl\}_3]^{2+}$		BNAH	DMF:TEOA 5:1	CO	0.093	240/15		16	≥ 500	69
23	$[(dmb)_2Ru(MebpyC_2Mebpy)Re(CO)_2\{P(p\text{-}FPh)\}_2]^{2+}$		BNAH	DMF:TEOA 5:1	CO	0.15	207/281		20	> 500	74
24	$[(dmb)_2Ru(tb\text{-}carbinol)\{Re(CO)_3Cl\}_2]^{2+}$		BNAH	DMF:TEOA 5:1	CO		190/11.8		16	≥ 500	71, 72
25	$[[(dmb)_2Ru]_2(tb\text{-}carbinol)Re(CO)_3Cl]^{2+}$		BNAH	DMF:TEOA 5:1	CO		110/6.9		16	≥ 500	52,53
26	p-terphenyl	$Co(cyclam)^{3+}$	TEOA	MeOH/MeCN 1:4	CO, H_2, $HCOO^-$	0.25 (CO + $HCOO^-$)			1	290	81
27	p-terphenyl	$Co(HMD)^{2+}$	TEOA	MeOH/MeCN	CO, H_2, $HCOO^-$				1	313	81, 83
28	Phenazine	$Co(cyclam)^{3+}$	TEA	MeOH/MeCN / TEA 10:1:0.5	CO, H_2, $HCOO^-$	0.07 ($HCOO^-$)			3	313	82
29	$Fe^{III}(TPP)$		TEA	DMF	CO		70		180	UV	85
30	$Co^{III}(TPP)$		TEA	MeCN	$HCOO^-$, CO		> 300 (total)		200	< 320	84

Table 1.2 Continued

	Chromophore	Cat/relay	Donor	Solvent	Product	Φ (mol/einsteins)	TON/ TOF	pH	Irr. time h	λ nm	Ref
31	{[Zn(TPP)]/[Re($CO)_3$ (pic)(bpy)]}		TEOA	DMF:TEOA 5:1	CO		30			>520	155
32	[Re(4,4'-$(MeO)_2$-bpy) $(CO)_3(P(OEt)_3)]^+$	[Re(bpy)($CO)_3$ $(CH_3CN)]^+$	TEOA	DMF:TEOA 5:1	CO	0.59			25	< 330	65
33	$ReCl(bpy)(CO)_3$		TEOA	DMF:TEOA 5:1	CO		27		4	> 400	64
34	$ReCl(bpy)(CO)_3$		TEA	DMF:TEA 0.8 M TEA	CO		8.2(Cl) 42(COO)		25		62
35	$ReBr(bpy)(CO)_3$		TEOA	TEOA:DMF 1:2	CO	0.15	20/5		11.7 min	436	57, 59, 64
36	ReOCHO(bpy)($CO)_3$		TEOA	TEOA:DMF 1:5	CO	0.05	12		20 min	> 330	64, 68
37	[Re(bpy)$(CO)_3(PR_3)]^+$		TEOA	DMF:TEOA 5:1	CO	0.38 (R=Oet), 0.013 (R=nBu), 0.024(R=Et), 0.2 (OiPr), 0.17 (R-Ome)	7.5/0.5 (R=Oet),1/ 0.1 (R=nBu), 6.2/0.5 (OiPr), 5.5/0.4 (R-Ome)		13	365	66, 156
38	[Re(bpy)$(CO)_3$ $(P(Ohex)_3)]^+$		TEA	CO_2(liquid)	CO		2.2/1.1		2	365	157
39	[Re(bpy)$(CO)_3(P$ $(OiPr)_3)]^+$		TEOA	DMF:TEOA	CO		15.6/0.7		24	365	158

Table 1.2 - Continued

	Chromophore	Cat/relay	Donor	Solvent	Product	Φ (mol/einsteins)	TON/ TOF	pH	Irr. time h	λ nm	Ref
40	$[Re(bpy)(CO)_3(4\text{-}X\text{-}py)]^+$		TEOA	TEOA:DMF 1:5	CO	0.03 (x=tBu, Me,H), 0.04 (x=C(O)Me), 0.13 (X=CN)	1/0.1 (x=tBu, Me,H, C(O)Me), 3.5/0.4 (X=CN)		8.5	365	159
41	$[Re(4,4'\text{-}(CF_3)_2\text{-}bpy)(CO)_3(P(OEt)_3)]^+$		TEOA	DMF:TEOA 5:1	CO	0.005	<1/<0.1		17	365	156
42	$[Re(dmb)(CO)_3(P(OEt)_3)]^+$		TEOA	DMF:TEOA 5:1	CO	0.18	4.1/0.2		17	365	156

1.3.2 Excited State Potentials for $Ru(phen)_3^{2+}$ Compared with CO_2 Redox Potentials

For photochemical reduction in homogeneous system, the chromophores $[Ru(phen)_3]^{2+}$ and $[Ru(bpy)_3]^{2+}$ still represent one of the most widely used systems for driving highly endogonic redox reactions, due to their excited state energetics and good

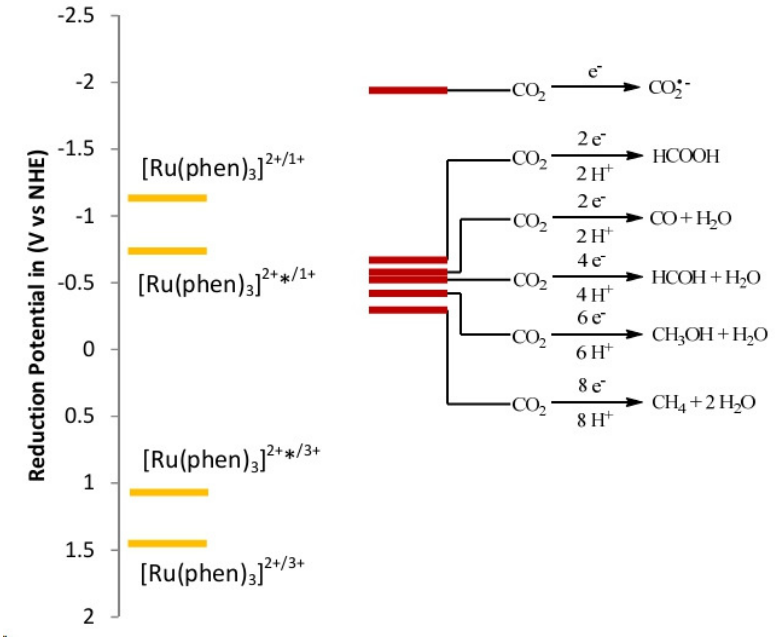

Figure 1.1 Reduction potentials of carbon dioxide reduction as compared with the excited state reduction potentials of $[Ru(phen)_3]^{2+}$.

chemical stability.[21] We make a particular point of introducing this chromophore as it and its analogs have been the primary chromophores used in studies on homogeneous photochemical reduction of CO_2. As shown schematically in Figure 1.1, the reduction potential for both the photoexcited state $[Ru(phen)_3]^{2+*}$ and the reductively quenched chromophore $[Ru(phen)_3]^{+}$ are negative of the key CO_2 reduction couples, meaning that these species are thermodynamically capable of reducing CO_2. The difficulty in using them is that they themselves lack the chemical functionality to lower the activation barriers involved and are only capable of delivering a single electron each towards these multi-electron reactions. It is also worth noting that the initial conversion of CO_2 to CO is

the energy “hog” in the overall process and consumes a minimum of 1.33 eV.[22] Much of the progress associated with the conversion of CO_2 to CO and formate has revolved around electro- and photocatalytic strategies for minimizing the additional overpotential over and above this minimum threshold.

This has led to the adaptation of many electrochemical catalysts to be used in conjunction with known chromophores to give new photochemical systems. These adaptations can resulted in both intermolecular systems, where both the chromophore and catalyst are dissolved into solution together, and intramolecular systems, where the electrocatalyst is attached covalently to the chromophore to allow for better transport of the electron between the two.

1.4 Electrocatalytic CO_2 Reduction with Molecular Catalysts

Many homogeneous catalysts have been developed for both electrochemical and photochemical systems; however, few are capable of deeper reductions than the two-electron reduced products of CO_2, such as CO and formic acid. Table 1.3 contains a collection of all (at least to the best of my knowledge) reported molecular electrocatalyst systems for CO_2 reduction in which the actual product of reduction was identified. The table includes information on the catalyst, electrochemical conditions, and products. Of the 72 entries in Table 1.3, 71 of these are metal complexes with the final product being a net two electron reduction of CO_2. The sole organic entry (#72), pyridine, is capable of catalyzing deeper reductions to products including methanol and is described in the next section. Metal phthalocyanines have also been reported tocatalyze the even deeper reduction of CO_2 to CH_4, but these are known to form electrochemically active films and thus are more of a heterogeneous catalyst.[23]

Table 1.3 Electrochemical systems for CO_2 reduction with reduction potentials, electrolyte, electrodes, electrolysis potentials with all potentials are reported in NHE except where noted.

	Catalyst	WE	Electrolyte	Solvent	Product	Efficency (%)	Redox Couple (V)	CO_2 reduction (V)	Notes	Ref
1	$[Co(salophen)]^{2+}$	Hg	$Li(ClO_4)$	MeCN	CO, CO_3^{2-}		-1.02	-1.29	TON >20	24-26
2	$[Fe^{3+}(dophen)Cl]_2$	GC	$TBAPF_6$	DMSO	CO, $HCOO^-$, $C_2O_4^{2-}$	18.5/67.2/ 9.8	-1.75	-1.69	improved by Li^+ and CF_3CH_2OH	27
3	$[Fe^{3+}(dophen)(N\text{-}MeIm)_2]_2$	GC	$TBAPF_6$	DMSO	CO, $HCOO^-$, $C_2O_4^{2-}$	13.3/73.6/ 7.3	-1.72	-1.69	improved by Li^+ and CF_3CH_2OH	27
4	$[Fe^{3+}(dophen)Cl]_2$	GC	$TBAPF_6$	DMF	CO, $HCOO^-$, $C_2O_4^{2-}$	22.5/57.2/ 13.4	-1.71	-1.69	improved by Li^+ and CF_3CH_2OH	27
5	$[Fe^{3+}(dophen)(N\text{-}MeIm)_2]_2$	GC	$TBAPF_6$	DMF	CO, $HCOO^-$, $C_2O_4^{2-}$	23.9/58.9/ 11.1	-1.72	-1.69	improved by Li^+ [28]and CF_3CH_2OH	27
6	$[Ni(cyclam)]^{2+}$	Hg	KNO_3	H_2O	CO	99	-1.33	-1.0	pH 4.1 4 h 18 TOF/77.5 TON	29-32
7	$[Ni(tmdnTAA)]^{2+}$	GC	TEtA (ClO_4)	DMF: H_2O 1:1	CO		-0.84	-1.60		33
8	$[Ni(HACD)]^{2+}$	Hg (HMD)	$Li(ClO_4)$	H_2O	CO		-1.12	-1.36		34
9	$[Ni(decyclam)]^{2+}$	Hg (HMD)	$Li(ClO_4)$	H_2O	CO, $HCOO^-$, H_2		-1.23	-1.36	pH 5.0	35
10	$[CHx(Ni(cyclam))_2]$	HMD	$TBAPF_6$	MeCN/ H_2O	CO,H_2		-1.21	-1.46		36

Table 1.3 - Continued

	Catalyst	WE	Electrolyte	Solvent	Product	Efficency (%)	Redox Couple (V)	CO_2 reduction (V)	Notes	Ref
11	$Co(dmg)_2(H_2O)Py$	GC	TMACl	EtOH	CO			-0.65	Temp 20-22 C	37
12	[Co(TPP)]	GC/ Pt	TBAF	DMF	$HCOO^-$	10	-0.53	-1.26		38-41
13	[Fe(TPP)]	Hg	TEtA (ClO_4)	DMF	CO	94	-1.41	-1.46	Mg^{2+}, or CF_3CH_2OH	42-45
14	$[Co(tpy)_2]^{2+}$	GC	TBA (ClO_4)	DMF	HCOOH		-1.46	-1.46	detected by chromotropic assay	46
15	$[Ni(tpy)_2]^{2+}$	GC	TBA (ClO_4)	DMF			-0.96	-0.96		46,47
16	$[Ni(bpy)_3]^{2+}$	GC	TBA (ClO_4)	MeCN	CO, CO_3^{2-}		-0.9	-0.90		48
17	$[Ru(bpy)_2(CO)_2]^{2+}$	Hg (HMD)	TBA (ClO_4)	H_2O: DMF 9:1	$HCOO^-$, CO	34/	-0.79	-1.26	pH 9.5/6.0, Temp 30 C 16 TON/12 TON	49,50
18	$[Ru(bpy)_2(CO)_2]^{2+}$	Hg	TBA (ClO_4)	MeOH	$HCOO^-$, CO, H_2	52.5/32.0	-0.79	-1.26		50-52
19	$[Ru(bpy)_2(CO)_2]^{2+}$	Hg	TBA (ClO_4)	MeCN	$HCOO^-$, CO, H_2	84.2/2.4/ 6.8	-0.79	-1.06	Me_2NH•HCl, Effiecency of $HCOO^-$ increases with increasing pk_a	50-53
20	$[Ru(dmbpy)(bpy)(CO)_2]^{2+}$	Hg	TBA (ClO_4)	MeCN: H_2O 4:1	CO	71.80	-0.89	-1.06		51
21	$[Ru(dmbpy)(bpy)(CO)_2]^{2+}$	Hg	TBA (ClO_4)	MeOH	CO, $HCOO^-$	34.2/39.8	-0.89	-1.06		51
22	$[Ru(dmbpy)_2(CO)_2]^{2+}$	Hg	TBA (ClO_4)	MeCN: H_2O 4:1	CO	65.30	-0.89	-1.06		51

Table 1.3 - Continued

	Catalyst	WE	Electrolyte	Solvent	Product	Efficency (%)	Redox Couple (V)	CO_2 reduction (V)	Notes	Ref
23	$[Ru(dmbpy)_2(CO)_2]^{2+}$	Hg	TBA (ClO_4)	MeOH	CO, $HCOO^-$	44.7/32.5	-0.89	-1.06		51
24	$[Ru(phen)_2(CO)_2]^{2+}$	Hg	TBA (ClO_4)	MeCN: H_2O 4:1	CO	61.5	-0.82	-1.06		51
25	$[Ru(phen)_2(CO)_2]^{2+}$	Hg	TBA (ClO_4)	MeOH	CO, $HCOO^-$	34.7/24.5	-0.82	-1.06		51
26	$[Ru(bpy)(Cl)_2(CO)_2]^{2+}$	Hg	TBA (ClO_4)	MeCN: H_2O 4:1	CO	87.80		-1.06		51
27	$[Ru(bpy)(Cl)_2(CO)_2]^{2+}$	Hg	TBA (ClO_4)	MeOH	CO, $HCOO^-$	27.3/37.7		-1.06		51
28	$[Ru(dmbpy)(Cl)_2(CO)_2]^{2+}$	Hg	TBA (ClO_4)	MeCN: H_2O 4:1	CO	66.00		-1.06		51
29	$[Ru(dmbpy)(Cl)_2(CO)_2]^{2+}$	Hg	TBA (ClO_4)	MeOH	CO, $HCOO^-$	39.2/26.8		-1.06		51
30	cis-$[Os(bpy)_2H(CO)]^+$	Pt_{mesh}	$TBAPF_6$	MeCN	CO	90	-1.10, -1.36	-1.16 to -1.36		54
31	cis-$[Os(bpy)_2H(CO)]^+$	Pt	$TBAPF_6$	MeCN 0.3 M H_2O	CO, $HCOO^-$	/25				54
32	$[Re(CO)_3(Cl)(bpy)]$	GC/Pt	TEtACl	DMF 10% H_2O	CO	98	-1.47	-1.25		55-57
33	$[Re(CO)_3(ClO_4)(bpy)]$	GC	$TBAPF_6$	DMF 10% H_2O	CO	99	-1.12	-1.25		55,56,58, 59
34	$[Re(CO)_3Cl(dmbpy)]$	GC	TEtA (BF_4)	MeCN	CO		-1.30	-1.52		60,61

Table 1.3 - Continued

	Catalyst	WE	Electrolyte	Solvent	Product	Efficency (%)	Redox Couple (V)	CO_2 reduction (V)	Notes	Ref
35	$[Re(CO)_3Cl(pbmbpy)]$	Pt_{mod}	TBA (ClO_4)	MeCN	CO, CO_3^{2-}	81	-1.72 vs Ag/10 mM Ag^+	-1.85 V vs Ag/10 mM Ag^+	14% oxalate	62
36	Re(tBu-bpy)$(CO)_3Cl$	GC	$TBAPF_6$	MeCN	CO	99	-1.59	-1.76		60
38	$[(\eta^6\text{-}C_6H_6)Ru(bpy)Cl]^+$	Pt		MeCN	CO, $HCOO^-$					63
39	cis-$[Rh(bpy)_2(CF_3SO_3)_2]^+$	Pt	$TBAPF_6$	MeCN	$HCOO^-$		-0.98, -1.27		40 to 100 minute run, 12.3 TON	63,64
40	cis-$[Ir(bpy)_2(CF_3SO_3)_2]^+$	Pt	$TBAPF_6$	MeCN				-0.96 to -1.36		63,64
41	$[Ni(MeCN)_4(PPh_3)]^{2+}$	GC	TBA (ClO_4)	MeCN	CO, CO_3^{2-}					48
42	$[Ni_3(\mu\text{-}CNMe)(\mu_3\text{-}I)(dppm)_3]^+$	Hg	$NaPF_6$	THF	CO, CO_3^{2-}		-0.89	-0.89		65
43	[Ru(terpy)(dppe)Cl]$^+$	Pt		MeCN	CO, $HCOO^-$					63
44	[RhCl(dppe)]	Hg	TEtA (ClO_4)	MeCN	$HCOO^-$	42	-1.52	-1.21	MeCN proton source	66
45	$[Ir(CO)Cl(PPh_3)_2]$	Hg	$TBABF_4$	DMF 10% H_2O	CO		-1.70	-1.06	Temp 20 C	67
46	$[Pd(PPh_3)(PPh_3)]$	GC	TEtA (BF_4)	MeCN + H^+	CO, H_2		-0.33			68
47	$[Pd(PPh_3)(PEt_3)]$	GC	TEtA (BF_4)	MeCN + H^+	CO,H_2		-0.69			68
48	$[Pd(PPh_3)(P(OMe)_3)]$	GC	TEtA (BF_4)	MeCN + H^+	CO,H_2		0.37			68
49	$[Pd(PPh_3)(P(CH_2OH)_3)]$	GC	TEtA (BF_4)	MeCN + H^+	CO,H_2		-0.51			68

Table 1.3 - Continued

	Catalyst	WE	Electrolyte	Solvent	Product	Efficency (%)	Redox Couple (V)	CO_2 reduction (V)	Notes	Ref
50	$[Pd(PPh_3)(MeCN)]$	GC	TEtA (BF_4)	MeCN + H^+	CO,H_2		-0.48			68
51	$[Pd(PPh_3)_2$ (2-m-8-Hq)]Cl	Pt	$TBAPF_6$	MeCN	CO	60.2		-0.94		69
53	$[Pd(PPh_3)_2$ (2-Qui)]Cl	Pt	$TBAPF_6$	MeCN	CO	56.7		-0.94		69
54	$[Pd(PPh_3)_2$ (2-Qui)]Cl	Pt	$TBAPF_6$	MeCN: H_2O 25:2	CO, $HCOO^-$	24.0/37.7		-0.94		69
55	$[Pd(PPh_3)_2$ (3-Hiq)]Cl	Pt	$TBAPF_6$	MeCN	CO	73		-0.94		69
56	$[Pd(PPh_3)_2$ (3-Hiq)]Cl	Pt	$TBAPF_6$	MeCN: H_2O 25:2	CO, $HCOO^-$	31.7/25.2		-0.94		69
57	$[Pd(PPh_3)_2$ (1-Hiq)]Cl	Pt	$TBAPF_6$	MeCN	CO	74.5		-0.94		69
58	$[Pd(PPh_3)_2$ (1-Hiq)]Cl	Pt	$TBAPF_6$	MeCN: H_2O 25:2	CO, $HCOO^-$	31.1/25.8		-0.94		69
59	$[Pd(PPh_3)_2$(2-m-1,10-phen)]$(ClO_4)_2$	Pt	$TBAPF_6$	MeCN	CO	60.9		-0.94		69
60	$[Pd(PPh_3)_2$(2-m-1,10-phen)]$(ClO_4)_2$	Pt	$TBAPF_6$	MeCN: H_2O 25:2	CO, $HCOO^-$	31.5/39.5		-0.94		69
61	$[Pd(PPh_3)_2$ (dmbpy)]$(ClO_4)_2$	Pt	$TBAPF_6$	MeCN	CO	81.0		-0.94		69
62	$[Pd(PPh_3)_2$ (dmbpy)]$(ClO_4)_2$	Pt	$TBAPF_6$	MeCN: H_2O 25:2	CO, $HCOO^-$	44.2/30.0		-0.94		69

Table 1.3 Continued

	Catalyst	WE	Electrolyte	Solvent	Product	Efficency (%)	Redox Couple (V)	CO_2 reduction (V)	Notes	Ref
63	$[Co(PPh_3)_2$(2-m-1,10-phen)$](ClO_4)_2$	Pt	$TBAPF_6$	MeCN	CO	62.6		-0.94		69
64	$[Co(PPh_3)_2$(2-m-1,10-phen)$](ClO_4)_2$	Pt	$TBAPF_6$	MeCN: H_2O 25:2	CO, $HCOO^-$	32.6/41.0		-0.94		69
65	$[Co(PPh_3)_2$ (dmbpy)$](ClO_4)_2$	Pt	$TBAPF_6$	MeCN	CO	83.4		-0.94		69
66	$[Co(PPh_3)_2$ (dmbpy)$](ClO_4)_2$	Pt	$TBAPF_6$	MeCN: H_2O 25:2	CO, $HCOO^-$	44.8/29.1		-0.94		69
67	$[Co(PPh_3)_2$ (2-m-8-Hq)]Br	Pt	$TBAPF_6$	MeCN	CO	61.4		-0.94		69
68	$[Co(PPh_3)_2$ (2-m-8-Hq)]Br	Pt	$TBAPF_6$	MeCN: H_2O 25:2	CO, $HCOO^-$	25.8/43.9		-0.94		69
69	$[Rh_2$ $(PhCHOHCOO)_2$ $(phen)_2(H_2O)_2]^{2+}$	Pt	TBA (BF_4)	DMF: H_2O 10:1	CO, $HCOO^-$	85-90	-0.55	-0.74		70
70	$[Fe_4S_4(SCH_2Ph)_4]^{2-}$	Hg	TBA (BF_4)	DMF	$HCOO^-$			-1.76		71
71	$[Fe_4S_4(SXN^-)_4]^{2-}$	Hg	TBA (BF_4)	DMF	$HCOO^-$	40/23		-1.80	X=-$COCMe^{2-}$, $COC_6H_4CH_2$	72
72	Pyridine	Pt/Pd/p-GaP	$Na(ClO_4)$	H_2O	HCOOH, MeOH	10.8/22	-0.34		pH 5.0, 30 - 50 μA	1,2,73

1.4.1 Pyridine for Electrocatalytic Reduction of CO_2

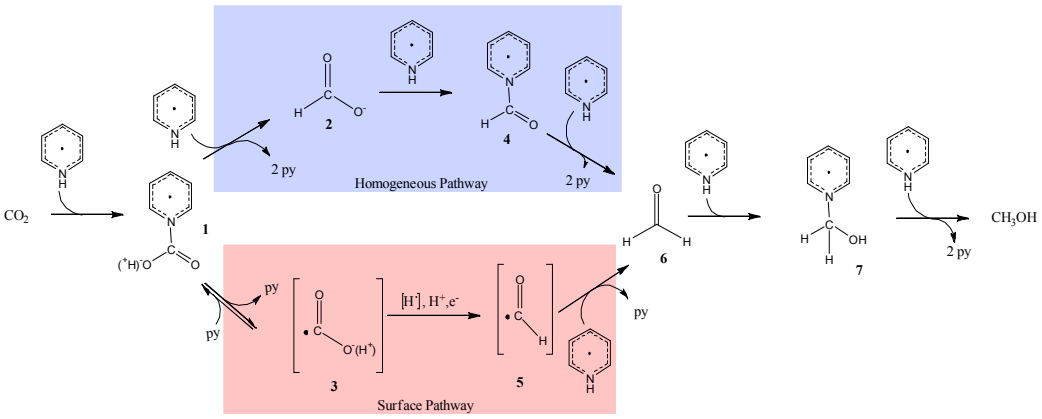

Figure 1.2 Pyridinium catalyzed reduction of CO_2 with the surface pathway in red and the homogeneous pathway in blue[1-3]

Bocarsly et al. has shown it is possible to reduce CO_2 to methanol by using a very simple electrocatalyst, pyridinium, which upon reduction can bind CO_2 to form carbamate-type adducts and, via redox cycling, shuttles six electrons to ultimately form methanol, as shown in Figure 1.2.[2] Through simulation of experimental results and kinetic studies, they were able to deduce the possible mechanism of the reduction of CO_2 to methanol.[24,74] The electron transfer in this process proceeds through an inner sphere electron transfer as was shown by $^{13}C^{15}N$ coupling in NMR and by gas-phase photoelectron spectroscopy.[1] Based on the calculated bond distance and bond angles the nature of the N-CO_2 bond was found to be primarily of π-character as opposed to σ-character. Reductions beyond the first electron transfer were found to depend on the electrodes being used.[1] For electrodes with low hydrogen potential, such as Pt or Pd, it was found that dissociation of the pyridine-formate radical adduct occurs, allowing the next reduction to formate/formic acid to take place on the electrode surface.[1] For electrodes with high hydrogen potential, the reaction is catalyzed entirely by the pyridinium with no dissociation of the formate radical, but a second pyridinium radical

passes an electron to the pyridine-formate radical adduct instead.[1,74] With low hydrogen potential electrodes, formic acid adsorbs onto the surface to produce the hydroxyformyl radical that reacts with a surface hydrogen atom to make the formyl radical which is finally reduced to the pyridinium radical to formaldehyde, bottom of Figure 1.2.[1] For high hydrogen potential electrodes, formic acid reacts withthe pyridinium radical to make the pyridinium-formyl adduct which is further reduced by a second pyridinium radical to form free formaldehyde and two equivalents of pyridine, top of Figure 1.2.[1] The reduction of formaldehyde for both electrode types results from the reaction with a pyridinium radical to form a pyridinium-formyl radical adduct, and this species reacts with a second pyridinium to produce methanol and two equivalence of pyridine.[1]

There is some debate about this mechanism proposed by Bocarsly et al. and with some groups claiming a non-innocent role of the surface in the process and thus a process which is necessarily heterogeneous.[1,24] Carter et al. claim that the reduction of CO_2 by a homogeneous pyridinium radical is not possible with the metallic surface being an absolute requirement. This paper was point for point debunked by Musgrave and coworkers who suggested a different method of this process taking place. Carter et al. followed this paper up with a recalculation of their work indicating that the pyridinium is reduced at one of the carbon atoms to form a dihydropyridine species that with the aid of the electrode's surface can reduce CO_2 to methanol.[75] The matter of the surface's effect remains without a definitive answer at this time.

1.4.2 Rhenium Polypyridyl Complexes for Electrocatalytic Reduction of CO_2

The highly selective and efficient nature of the *fac*-Re(bpy)$(CO)_3$X (X = Cl, Br) has driven the large amount of research activity of this complex towards electrochemical CO_2 reduction.[15,17,55,56,59-61,76,77] The catalytic reduction can proceed through two different pathways: a one-electron or a two-electron pathway (Figure 1.3), both of which yield CO.[56] The one-electron pathway (Figure 1.3, left), the coordinatively unsaturated Re(0) species binds CO_2 to give the equivalent of a bound $CO_2^{\cdot-}$ radical anion, which upon

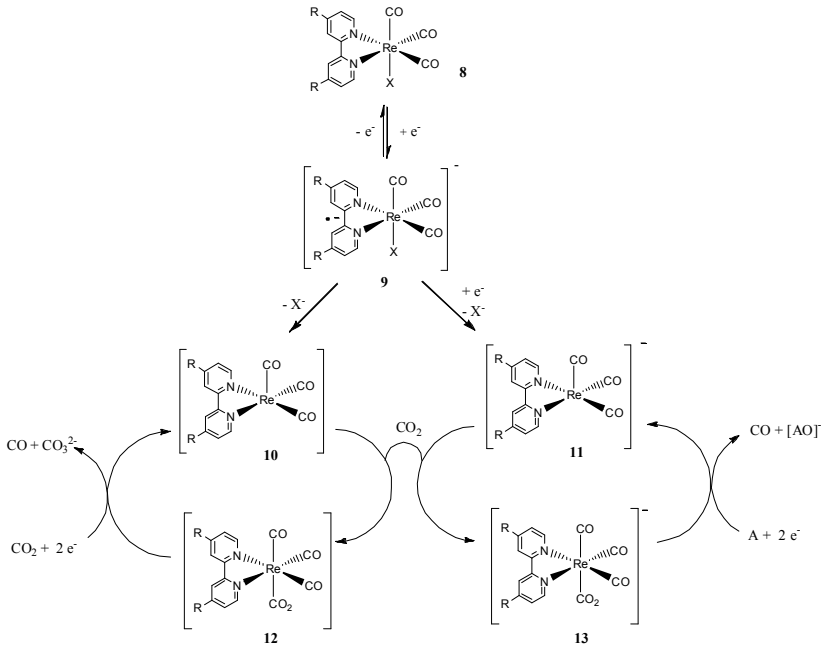

Figure 1.3 The proposed one-electron and two-electron pathways.

reaction with another $CO_2^{\cdot-}$ radical anion (CO_2 and a second electron) disproportionates to yield CO and CO_3^{2-}.[78,79] In the two electron pathway (Figure 1.3 right), the starting complex is reduced twice and upon loss of the halide, yield a coordinatively unsaturated Re(-1) complex. Binding of CO_2 and in the presence of some oxide acceptors, such as H^+, yields CO and H_2O.[15,56]

Both of these pathways, the one-electron and two-electron, are accessible with the same complex but at different potentials. Based on the work published by Meyer et al. species **9**, the one-electron reduced species, is formed at -1.11 V versus NHE.[56] Under Ar, this couple is also associated with the formation of a Re-Re dimer, [*fac*-Re(bpy)$(CO)_3]_2$, which has been implicated as the reactive species in some works.[56,61] The second reduction of *fac*-[Re(bpy)$(CO)_3X]^-$ is observed at –1.26 V vs. NHE and can also result in halide loss and generation of the active catalyst.[15] At a higher potential of -1.56 V vs. NHE the system proceeds through the two-electron reduction pathway as shown on the right side of Figure 1.3 to give CO without the formation of carbonate.[56] Studies by Kubiak et al have shown that by changing the 4,4' substituents on the bpy-ligand in *fac*-Re(bpy)$(CO)_3$X it was possible to enhance the electrocatalysis reaction rate from 50 $M^{-1}s^{-1}$ for H to 1000 $M^{-1}s^{-1}$ for the *t*-Bu derivative as well as to increase the Faradaic efficiency (~99%).[60]

1.4.3 Ruthenium Polypyridyl Complexes *for Electrocatalytic Reduction of* CO_2

Other than rhenium-based complexes, ruthenium polypyridyl complexes are the next most well explored. $Ru(phen)_2(CO)_2^{2+}$ and $Ru(bpy)_2(CO)_2^{2+}$ are reported to reduce CO_2 electrocatalytically. These complexes typically make CO, H_2, and formate as products of reduction,[49,51,52,80-84] with the ratio of these products being pH dependent.[81,82] At pH 6, the products are CO and H_2; however at pH 9.5, formate is produced in addition to CO and H_2.

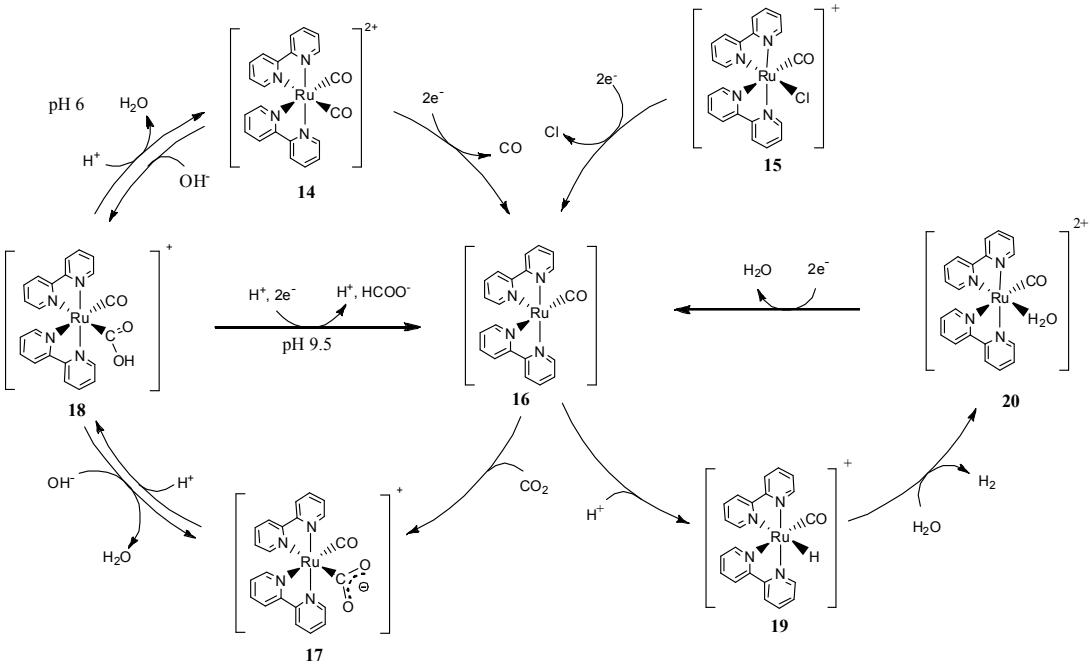

Figure 1.4 Tanaka's proposed electrocatalytic reduction of CO_2 by $[Ru(bpy)_2(CO)_2]^{2+}$ with possible pathways for CO, formate and H_2 formation.

Two different catalytic pathways have been proposed: the one theorized by Tanaka et al. and is shown in Figure 1.5,[53,81,82] and another by Meyer et al. and is shown in Figure 1.5.[11] Both discuss the reduction and loss of CO to form a neutral, coordinatively unsaturated $Ru(L\text{-}L)_2(CO)$ (**16**) species. Tanaka et al. can start with the dicarbonyl, species **14**, or the monocarbonyl monochloride, species **15**.[53,81,82] where the electrons are thought to sit on the bpy ligands.[11] Tanaka proposes that **16** can react with either CO_2 or H^+ to form one of two intermediates, the formato species **17** or the hydride species **19**.[53,81,82] The species **17** reacts with a proton to form the metallo-carboxylic acid (species **18**), which at pH 6 and reforms the dicarbonyl complex **14** but at pH 9.5, adds two electrons to produce formate and **16**.[53,81,82] Hydrogen is explained via the formation of the hydride in a competing side reaction.

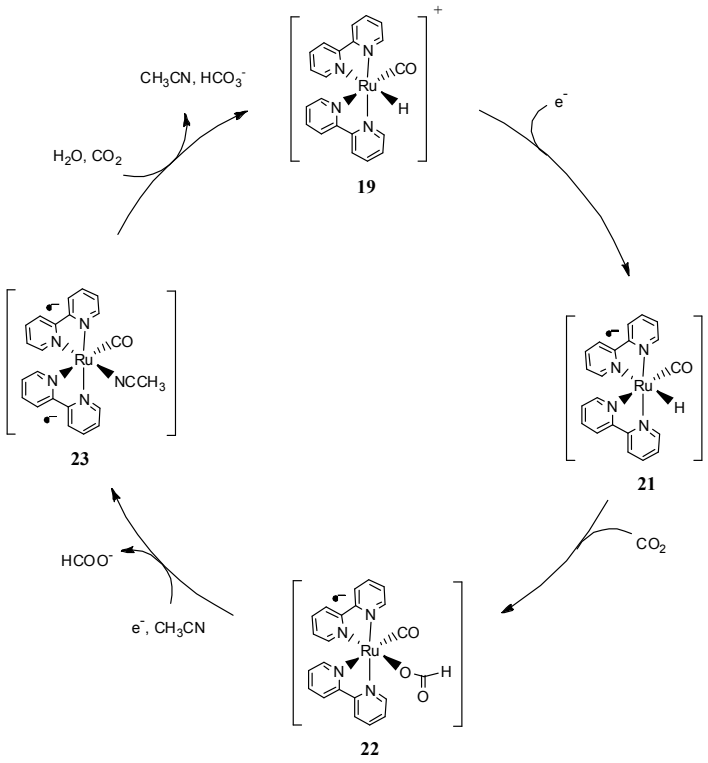

Figure 1.5 Meyer's proposed electrochemical reduction of CO_2 via hydride bond insertion to form formate

As shown in Figure 1.5, Meyer et al. proposes that the hydride species **19** is directly involved in the CO_2 fixing cycle and that after reduction to **21**, insertion of CO_2 into the metal hydride bond forms the formato-complex (species **22**).[11,54,85,86] Another reduction releases formate and generates a solvate complex which reacts with water to reform the hydride **19**.[86] Though there is no direct evidence for the formation of species **23**, and the catalysis could proceed through a system that goes directly from species **22** to species **19** with loss of formate and reduction of water in one step.[86]

1.6 Transition-Metal Complexes for Photocatalytic CO_2 Reduction

1.6.1 Catalysts for Reduction of CO_2 to CO or $HCOO^-$

Compared to the number of electrocatalysts for CO_2 reduction, photochemical catalysts are far more limited and are largely limited to Re and Ru complexes Table 1., to the best of our knowledge, contains a collection of all reported molecular photocatalytic systems for CO_2 reduction. Of the 42 systems reported, only 5 systems do not involve

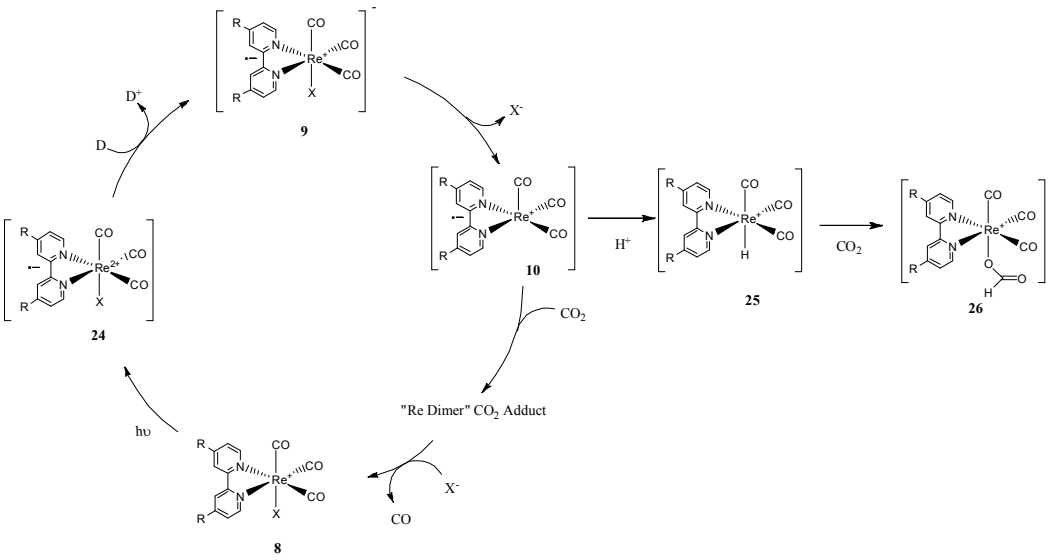

Figure 1.6 Photocatalytic cycle of *fac*-Re(bpy)$(CO)_3$X with the formation of the formate adduct.

Re or Ru. Three utilize the organic chromophores phenazine and para-terphenyls and two utilize Fe- and Co-based porphyrins. In most cases, the chromophore is coupled with a CO_2-reducing co-catalyst which is a known electrocatalyst for CO_2 reduction. CO, formate, and H_2 are the only reported products for these systems, with the sole exception of entry #15, indicating that deeper reduction has remained an elusive goal. In most of these systems, CO formation is proposed to occur via the disproportionation of the $CO_2^{\cdot-}$ radical anion[79] or a two-electron reduction to produce CO.[87-91]

One of the better studied photocatalysts is *fac*-[Re(bpy)$(CO)_3X]^+$ which is also one of the few systems in which the chromophore is also the CO_2 reducing catalyst. Hori[92] and Lehn[55,58,93] have proposed the mechanism shown in Figure 1.6 for the production of CO. After reductive quenching of the photoexcited state (**24**), dissociation of the halide forms the coordinatively unsaturated species **10** which then can react with CO_2. While the exact structure of the CO_2 complex is not fully known, one proposed structure is the μ_2-η^2-CO_2 bridged binuclear Re adduct.[55,58,92,93] In any case, the CO_2 adduct is unstable and decomposes to yield CO and **8**. Ishitani proposes a similar mechanism except that **10** adds CO_2 and instead of dimerization as a method to provide a second reducing equivalent, the CO_2 adduct is reduced a second time by an outer-sphere mechanism to yield CO and complex **8**.[94] At present, both mechanisms have reasonable data to support their claims.[56] Among a related rhenium photocatalyst family, *fac*-[Re(bpy)$(CO)_3P(OEt)_3]^+$ has been demonstrated to be most efficient.[90,95-97] The one electron reduced species is almost quantitatively produced and is unusually stable in solution because of the strong electron-withdrawing property of the $P(OEt)_3$ ligand.[90,95-97] A competing reaction in this system is the reaction of species **10** with a proton to give the metallo-hydride (species **25**).[55] This species can react with a proton to give hydrogen gas,[55] or it can insert CO_2 to give the metallo-formate complex (species **26**), which kills the catalyst as the formate is not released.[55,58] Hori and coworkers noted that it was possible to prevent this deactivation pathways, i.e. inhibit hydride formation, by increasing the CO_2 partial pressure.[92] Catalyst turnover exhibited a 5-fold improvement at 54 atm over a 1 atm system. One issue with the Re photocatalysts is the limited range of absorption in the visible region, which is typically limited to wavelengths below 440 nm. Multinuclear metal supramolecular complexes were developed for CO_2 reduction photocatalysts for this reason. These complexes were composed of a photosensitizer

part, a ruthenium(II) bpy-type complex, and a catalyst part based on the of rhenium(I) tricarbonyl complexes. A number of bi-, tri-, and tetra-nuclear complexes linked by several types of bridging ligands have been investigated in the literature (Figure 1.7).[90,98-103] The bridging ligands strongly influence photocatalytic ability, including selectivity of CO over H_2, high quantum yields and large turn over numbers, of the complexes. In all of these complexes, the ^{3}MLCT excited state of the ruthenium moiety was reductively quenched by a sacrificial reducing agent and the one electron reduced Re complex was formed through intramolecular electron transfer from the reduced Ru chromophore.[90]

Ishitani et al have shown that the catalytic activity of these mixed Re/Ru assemblies improves upon increasing the Re/Ru ratio, presumably due to the ready availability of Re sites (which catalyzes the slow step) to pick up electrons from the photoreduced Ru site (the fast step).[98,100,101] Moreover, a comparison of each multinuclear system to their corresponding system composed of the individual components shows that the intramolecular system is superior.[98-100] The electronic structure of the bridging ligands is important and systems in which there is strong electronic communication between metal sites perform less well than those with weak electronic coupling.[98,99] Thus, the more conjugated bridging is not better for supramolecular architecture for photochemical CO_2 reduction.[102] In order to direct the electron towards the Re center in the Ru/Re assemblies, it is important to adjust the π* orbital energy on peripheral bpy ligands of the Ru chromophores, such that they do not become electron traps.[98] Ideally, the acceptor orbital of the bpy-like portion of the bridging ligand should be equal or lower in energy than that of the peripheral ligands to help direct the electron to the Re site.[90,98]

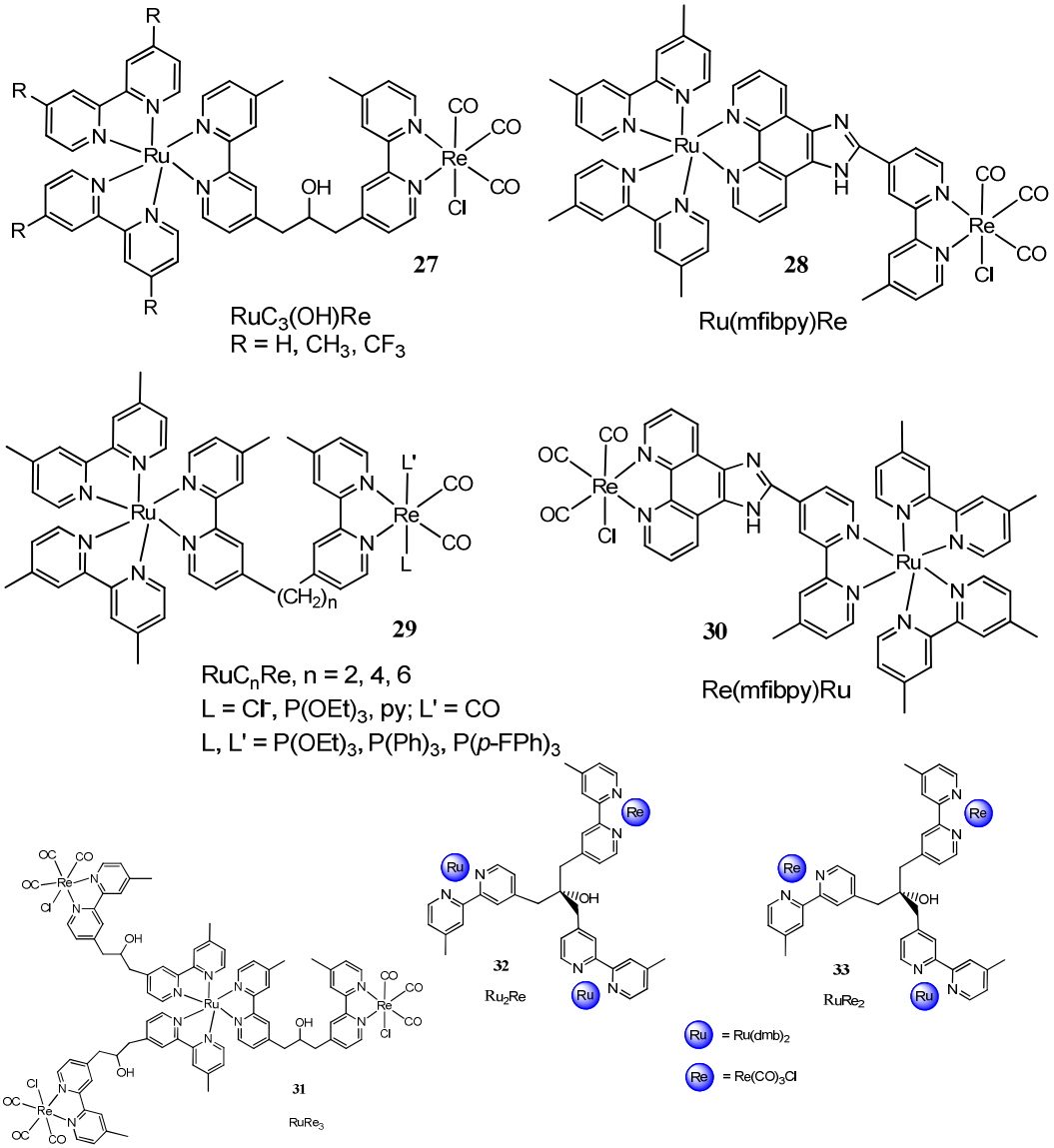

Figure 1.7 Chemical structures of multinuclear rhenium complexes.

Cyclam-based macrocyclic ligands with either cobalt or nickel ions are one of the most commonly used co-catalysts for the photochemical reduction of CO_2 in the

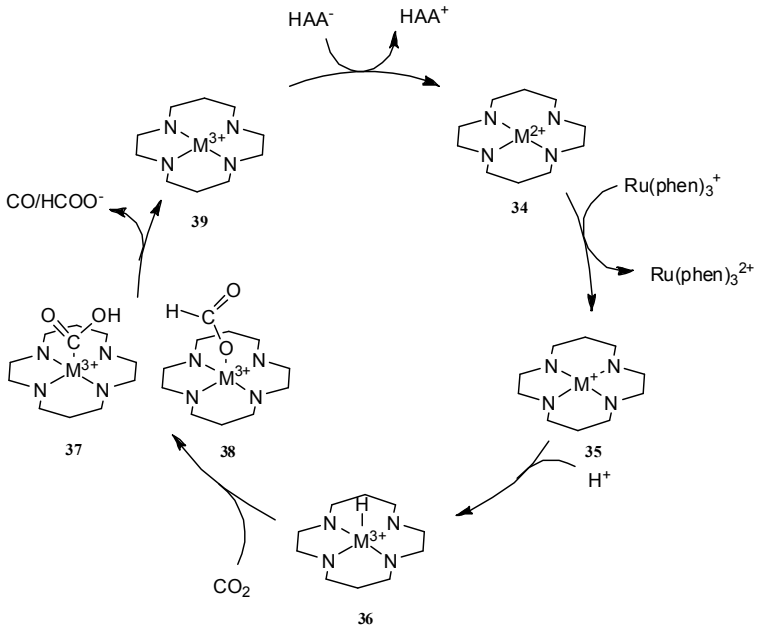

Figure 1.8. Acid assisted CO_2 electroreduction by metal cyclam where M is cobalt or nickel.

presence of $Ru(bpy)_3^{2+}$.[104-112] As seen in Figure 1.8,[107] the production of CO is shown to proceed through the reduction of the macrocycle by the singly reduced Ru species, $Ru(bpy)_3^{+}$, followed by formation of metal hydride intermediate (species **36**). The next step is insertion of CO_2 into the metal hydride bond to form the metallo-formate (**37**). This species then decomposes to form CO and water. This species can rearrange to for the oxygen-bound formate species **38** which can be lost as formate by simple protonation.[39,104,106,107,111] In both cases, the catalyst is regenerated by a reducing agent. A competing pathway in this system is the reaction between the metal hydride and another proton to form H_2. The use of a different photosensitizer yields an additional product with these catalysts. When *p*-terphenyl[110,112] or phenazine is used in place of $Ru(bpy)_3^{2+}$ the formation of formate is also observed in addition to CO and H_2.

Another class of macrocycle complexes that are used in the reduction of CO_2, are porphyrin-based complexes using iron and cobalt. The photochemical reduction of CO_2 with iron porphyrins, follows a similar catalytic process as the electrochemical reduction,

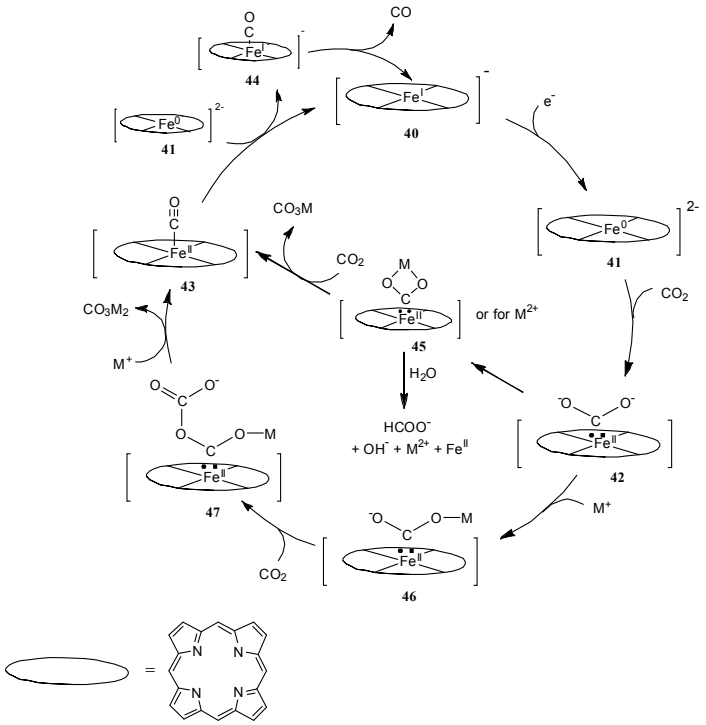

Figure 1.9 Metal ion-assisted CO_2 reduction where the metal ion is Ca^{2+}, Mg^{2+}, Na^{+}, Li^{+}, with Mg^{2+} working the best.

shown in Figure 1.9, with the key difference being the method in which the active species, $[Fe(0)TPP]^{2-}$, is formed.[113] In the photochemical method, the active species is formed through a three-step process which involves four photons and two porphyrin rings. The first step (Eqn. 8) is photoreduction of the iron(III) porphyrin to iron(II) porphyrin in the presence of a reducing agent, TEA, which is coordinated to the axial site of the complex.

$$\text{TEA-Fe(III)TPP} \xrightarrow{h\nu} \text{Fe(II)TPP} + \text{TEA}^{\bullet+} \quad (8)$$

$$\text{TEA-Fe(II)TPP} \xrightarrow{h\nu} \text{Fe(I)TPP}^{-} + \text{TEA}^{\bullet+} \quad (9)$$

$$2\ \text{Fe(I)TPP}^{-} \longrightarrow \text{Fe(0)TPP}^{2-} + \text{Fe(II)TPP} \quad (10)$$

The second step is further illumination of the iron(II) species to result in iron(I) species with a mechanism similar to first step (Eqn. 9). This process is far less efficient than the previous one and is affected by the concentration of TEA.The last step to make the active species of this complex is a disproportionation reaction of two iron(I) species in solution to give one iron(0) species and one iron(II) species (Eqn. 10). CoTPP, was demonstrated to perform similarly to FeTPP with $Co(0)TPP^{2-}$ as the active catalytic species.[39]

1.7 Concluding Remarks and Future Directions

The progress in the realm of molecular catalysts in the last 40 years toward the reduction of CO_2 has been substantial, but primarily limited to reduction to CO or formate. CO does have value in that it can be used in a Fischer–Tropsch reaction to produce higher carbon fuel products, however there is a general recognition that deeper reduction to more value-added products such as methanol are needed.

Although there are promising examples in the literatures, some obvious problems remain. The current state-of art does not meet the grand goal for industrial large-scale operation. The challenge to overcome is the overpotential for the electrochemical systems and short-lived one-electron reduced species for the photochemical systems. It is also critical to replace sacrificial reducing agents with more practical donors such as water, so as to close the loop in a practical fuel cycle. The use of sunlight to drive photoreduction is a sustainable method for the use of CO_2 as a C1 feedstock. Examples

of incorporation of a chromophore with the real catalyst in either intermolecular or intramolecular photochemical system have shown the feasibility of CO_2 reduction. However, photoinduced electron transfer from the chromophore to the catalyst or from the semiconductor to the solution still accounts for much of the inefficiency in these systems. To address this issue, it will require sustained efforts by scientists in the rational design of molecule- or semiconductor-based assemblies to reduce these inefficiencies.

Chapter 2

PHOTOCHEMICAL REDUCTION OF CARBON DIOXIDE TO METHANOL IN A HOMOGENEOUS WITH PYRIDINIUM CATALYSTS

2.1 Introdution

Photochemical, photoelectrochemical, and electrochemical processes for the reduction of CO_2 into fuel could play important roles in addressing current environmental and energy challenges associated with the continued use of fossil fuels.[114-126] Transition metal-based catalysts have been the focus of most homogeneous CO_2 reduction processes. Meyer and co-workers were one of the first to demonstrate that Rh and Ir polypyridyl complexes are competent electrocatalysts for CO_2 reduction in DMF under air-free, but ambient conditions.[64] Since then, there have been significant contributions in both electrocatalytic and photocatalytic CO_2 reduction with homogeneous catalysts by a number of groups including Meyer,[28,85,86,127-129] Fujita,[18,130,131] and others.[99,118,132-138] Notably, despite all the advances with CO_2 electro- and photoreduction with homogeneous transition-metal catalysts, products have been largely limited to the two-electron reduction products (CO or formic acid) with only a few accessing deeper reduction to CH_3OH or CH_4.[17,139] Methanol is a particularly attractive product in that it is a liquid under ambient conditions and can be readily integrated into the existing liquid fuel transportation infrastructure.[115,140] Solar-powered photochemical reduction of CO_2 to liquid fuels would be a particularly attractive and environmentally benign technology, as it could, in theory, lead to a carbon-neutral fuel cycle.

Despite the promise of such technology, there is only one known selective electrocatalyst for CO_2 to methanol, which is the surprisingly simple pyridine molecule. Bocarsly and co-workers have shown that pyridine, at pH 5, will selectively reduce CO_2 to methanol in a series of one-electron steps and at low overpotentials.[2,73,114,119] Other deep

reduction products such as formaldehyde or higher alcohols are only produced in trace quantity. While mechanistic studies are incomplete, evidence points to the formation of a carbamate-type intermediate between the CO_2 and a pyridinium radical and subsequent sequential electron and proton transfer processes to ultimately yield methanol.

The electrode surface appears to be intimately involved in the reduction mechanism as only Pt or Pd electrodes are active in electrocatalytic systems[141] and p-type GaP in photoelectrochemical systems.[73] It is clear that there is a significant positive shift in the pyridinium reduction potential (E_{red} = -0.34 V vs NHE)[119] when Pt and Pd electrodes are used compared to Hg electrodes (E_{red} = -0.95 V vs NHE)[142] and theoretical calculations of E_{red} = -1.1 V vs NHE.[141] This unusual positive shift with Pt and Pd electrodes has been used to support the argument that the surface is involved in the CO_2 reduction mechanism (beyond simply supplying electrons). It is notable that other working electrodes, such as glassy carbon or Hg, do not drive the pyridine-catalyzed CO_2 to methanol reduction even at more negative potentials.[142] These data suggested that homogeneous pyridine-based reduction of CO_2 to methanol may not be possible and the performance of the pyridine-based system would be tied to issues such as electrode surface area and composition. We sought to address this issue and ideally directly couple this system with solar energy by examining a homogeneous photochemical system in which the electrode is replaced by a homogeneous visible-light chromophore and electrons are supplied, in this case, by a sacrificial donor (ascorbate).

2.2 Results and Disscussion

Herein, we report on the homogeneous photochemical reduction of CO_2 to formic acid, and to a lesser extent, methanol, using pyridine as the CO_2 reducing catalyst and $[Ru(phen)_3]^{2+}$ as the chromophore. This complex and the closely related $[Ru(bpy)_3]^{2+}$ complex are well-known photosensitizers for photochemical reduction and oxidation

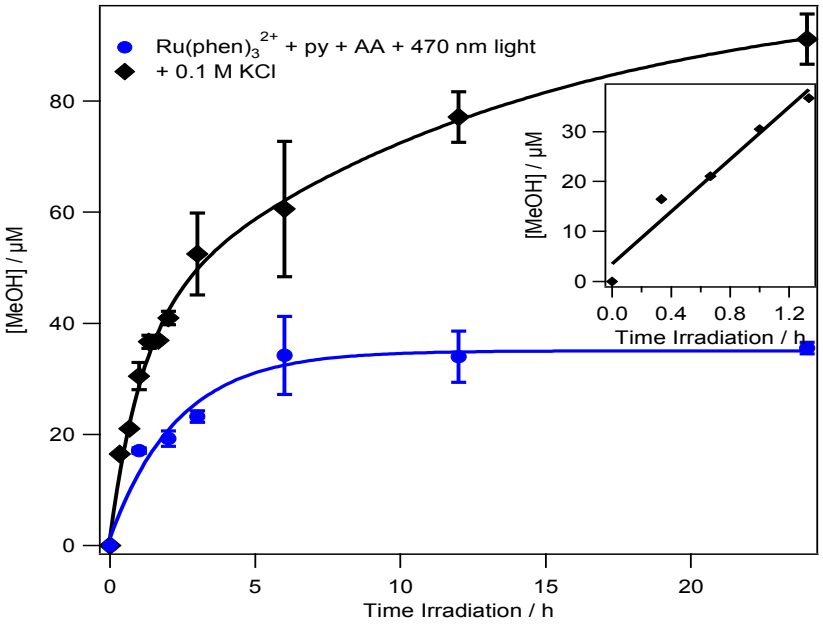

Figure 2.1 Growth of methanol with irradiation time for a solution (blue circles) 50 mM pyridine, 0.20 mM $[Ru(phen)_3]Cl_2$, 0.2 M ascorbic acid, at pH 5.0, 25.0 C and irradiation with 470 nm light. Black Diamonds: Performance of the same system with the additional component of 0.1 M KCl. The inset shows the initial growth of methanol for the first 1.3 hours of irradiation in the system with KCl where methanol production is linear.

reactions. Both possess strong MLCT absorptions in the 400-500 nm region which yield long-lived ^{3}MLCT states that transiently localize the electron on one of the phen or bpy ligands and the hole on the metal center {i.e., $[Ru^{III}(phen)_2(phen^{\cdot-})]^{2+*}$} to form a powerful excited state oxidant and reductant.[143,144] As shown in the black line in Figure 1, irradiation of a CO_2 saturated, aqueous solution of pyridine (50 mM), $[Ru(phen)_3]Cl_2$ (0.20 mM), 0.1 M KCl, and ascorbic acid (0.2 M), at pH 5.0 and 25.0 C at 470 (± 20 nm) in a custom-built LED photoreactor (see Supporting Information) steadily produces methanol for a 3 to 4 h period, after which activity falls off. While formic acid was the dominant product, we focused our initial optimization studies exclusively on methanol as this is the more desirable product. Methanol was detected by taking aliquots at various time points and analyzing for methanol by GC-MS. Samples were trap-to-trap distilled to remove all

Table 2.1 Optimization of $[Ru(phen)_3]^{2+}$ to pyridine ratio for methanol production

			MeOH			Formate		
Ru:py	n	pH	μM[a]	TON MeOH[a] (in e^-)	Φ[c] 10^{-5}	mM[b]	TON Formate (in e^-)[b]	Φ[c] 10^{-3}
2:1	1	5.0	0.00 ± 1	0.0	0.0	4.7	19 (39)	1
1:1	1	5.0	6.3 ± 2	0.03 (0.19)	0.75	2.6	11 (22)	0.6
1:2	1	5.0	6.1 ± 1	0.03 (0.18)	0.46	0.42	1.8 (3.6)	0.1
1:100	1	5.0	29 ± 3	0.14 (0.87)	2.6	0.26	1.0 (2.0)	0.06
1:200	3	5.0	31 ± 3	0.15 (0.92)	6.3	2.2	9 (18)	3
1:200 (0.1 M KCl)	3	5.0	66 ± 12	0.33 (2.0)	11	18	76 (152)	25
1:200 (pH 4.0)	2	4.0	0.00 ± 2	0.0	0.0	2.9	12 (24)	4
1:200 (pH 6.0)	2	6.0	13 ± 0.3	0.05 (0.31)	2.7	1.1	4.5 (9.0)	0.9

Conditions: pH 5.0, 0.20 mM $[Ru(phen)_3]^{2+}$, 0.1 M ascorbic acid, CO_2, py redistilled. [a] After 6 h irradiation, methanol as a function of ruthenium with electrons as a function of ruthenium in parentheses. [b]After 1 h irradiation, formate as a function of ruthenium with electrons as a function of ruthenium in parentheses. [c] □ reported on a per electron basis as a function of the slope of the initial linear portion of the product vs time plot.

Table 2.2 Runs of photolysis system with various metal co-catalysts

Co-catalyst	MeOH μM	TON MeOH:Ru	TON MeOH:e$^-$	Φ (10^{-5})
Pt/CB	30 ± 3	0.15	0.91	2.1
Pt colloid	0	-	-	-
Pd/CB	32 ± 1	0.16	0.97	2.2
Ni/CB	16 ± 0.8	0.08	0.48	3.8
Au/CB	13 ± 7	0.06	0.40	3.3

Conditions: pH 5.0, 0.20 mM $[Ru(phen)_3]^{2+}$, 40 mM pyridine, 0.1 M ascorbic acid, 0.08 mg/mL ~45% - 50% metal catalyst on carbon black support or 0.01 mg/mL colloidal Pt.

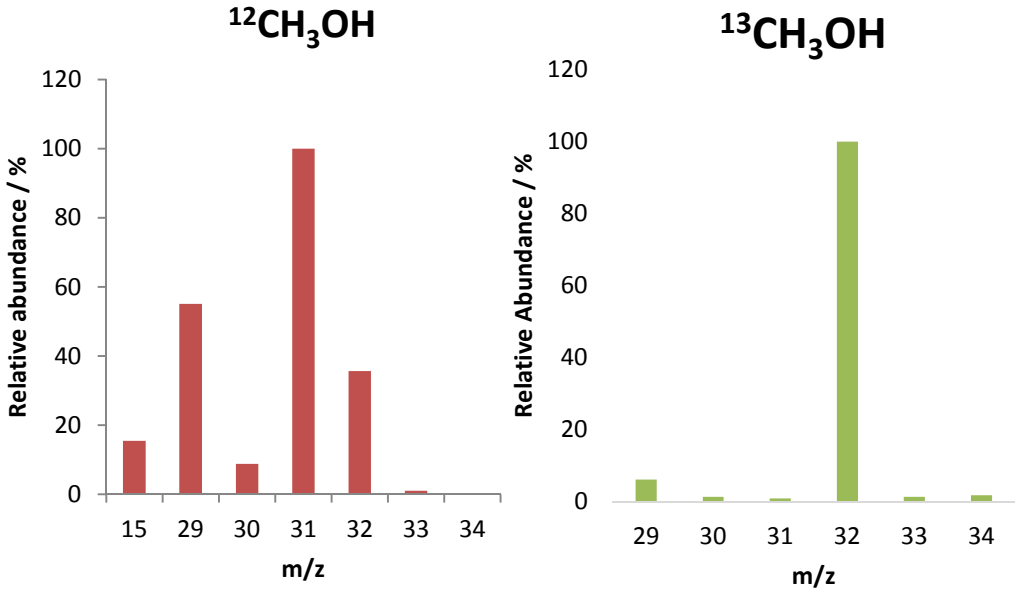

Figure 2.2 Mass spectrum of methanol produced from natural abundance CO_2 (red) and ^{13}C methanol produced from 99 % isotopically enriched $^{13}CO_2$ (green).

salts prior to GC-MS. Attempts to use ion-exchange resins for desalting[73] gave spurious peaks in the GC which interfered with the analysis. Methanol was detected at a m/z of 31 using single ion mode. Experiments using isotopically labeled $^{13}CO_2$ (99 % enriched) gave $^{13}CH_3OH$ confirming that the CO_2 is the carbon source for methanol production (see Figure 2.2).

Formic acid as formate was also detected by addition of strong base to the solid residue from the trap-to-trap distillation and removal of all volatiles under high vacuum. Dissolution in D_2O and NMR analysis with an internal standard (DDS) revealed considerable quantities of formate, as indicated in Table 2.1 (TON > 1). Quantitative analysis of formaldehyde was not possible due to interferences and difficulties in its isolation and detection, but NMR data suggest that it is only present in trace quantities at best. Control reactions established that all components, except KCl, were required for methanol production (see Table 2.3). The presence of KCl doubles the methanol production, but it is not absolutely required. Its role in this process is discussed later.

As seen in Table 2.1, the pyridine to chromophore ratio was found to be an important factor, with no methanol detected after 6 h irradiation when the chromophore was in excess, approximately 6 μM methanol detected when the ratio was 1:1 or 2:1, and on the order of 30 μM when pyridine was present in large excess (i.e., 1:100). When converted to turnover numbers (TON), this amounts to ~ 0.15 methanol per $[Ru(phen)_3]^{2+}$ or 0.9 electrons per $[Ru(phen)_3]^{2+}$, the latter being based on the six electron stoichiometry for the reaction. The reproducibility was good with the methanol concentration measured at 31 ± 3 μM after 6 h irradiation for three separate runs.

Table 2.3 Methanol production under changes to various system components.

Run	MeOH μM	TON MeOH:Ru	TON MeOH:e^-	ϕ ($x10^5$)
$Ru(phen)_3^{2+}$, AA, Py, KCl, CO_2, hν	66 ± 12	0.33	2.0	11
EVERYTHING EXCEPT:				
KCl	30 ± 3	0.15	0.92	6
hν (dark reaction)	0.0	-	-	-
Pyridine	0.0	-	-	-
ascorbic acid	0.0	-	-	-
$[Ru(phen)_3]Cl_2$	0.0	-	-	-
CO_2	0.0	-	-	-
pyridine changed to 4,4'-bpy (200:1 ratio)	0.0	-	-	-
pyridine changed to 4-cyanopyridine (200:1 ratio)	0.0	-	-	-
ascorbic acid changed to				
TEOA (pH 7.4)	0.0	-	-	-

In addition to methanol, formate was also observed in large quantities by NMR in D_2O, by comparing the peak area of the formate peak with that of an internal standard (DSS) it was determined that in the photolysis with the K^+ ion present ~27 mM formate was produced giving ~150 formate per $[Ru(phen)_3]^{2+}$ and ~230 formate per electron within the first hour of photolysis. This also greatly increases the quantum yield to 0.02 indigating a buildup of formate/formic acid after just one hour. With no trace of

formaldehyde and only an increasing methanol concentration would imply that the steps following formic acid reduction are fast, preventing a buildup of formaldehyde. This supports that reduction of formate/formic acid is RDS for this process, which is similar to what Borcarsley et al. observed.[1]

As with the electrochemical systems, the pH was important with optimum methanol production occurring around the pK_a of pyridinium ion (5.3), suggesting both the protonated and deprotonated pyridine are important for the overall process. As shown in Table 2.1, the optimum pH was 5.0 with no methanol production at pH 4.0 and a significant drop-off in methanol production at pH 6.0. The lack of methanol production at pH 4.0 may be due, in part, to the protonation of the ascorbate present (pK_a ascorbic acid = 4.1), as the ability of ascorbic acid to function as a sacrificial donor is less than that of ascorbate.[107,145,146] The use of a sacrificial donor is a temporary solution to any practical photochemical system but, as it is necessary here, the tight pH range limits the acceptable sacrificial donors to ascorbate as the more commonplace donors, such as organic amines, are generally protonated and inactive at these pHs.

It was noted that the electrolyte in the electrochemical systems was usually 0.1 to 0.5 M KCl and decided to see if the electrolyte composition had any effect, beyond simply providing a conductive solution, on the methanol production. The presence of potassium ion (KCl 0.1 M) dramatically increased the formate yield (8 X) and doubled the methanol yield after 6 hours in the photochemical system as seen in Table 2.1 and Figure 2.1 compared to the electrolyte free reactions. Saveant and Darensbourg[43,147] have shown in separate systems that ion-pairing between carboxylate functions with alkali and alkali-earth metal cations can stabilize the transition states involving CO_2 reduction in transition metal complexes coordinating a CO_2 ligand. In our case, the enhanced catalysis was

specific for potassium ion as addition of other salts, including LiCl, NaCl, RbCl, CsCl, and MgCl2 had little to no effect (see Table 2.4).

Table 2.4. Methanol production after 6 hours of irradiation with various salts. Quantum yields were calculated based on initial slope of methanol production.

Run	MeOH mM	TON MeOH:Ru	TON MeOH:e^-	Φ ($x10^{-5}$)
$Ru(phen)_3^{2+}$, AA, Py, CO_2	30 ± 3	0.15	0.92	6.3
+ 0.1 M LiCl	30 ± 0.9	0.15	0.91	4.3
+ 0.1 M NaCl	30 ± 3	0.15	0.90	7.1
+ 0.1 M KCl	66 ± 12	0.33	2.0	11
+ 0.1 M RbCl	24.6 ± 0.3	0.12	0.74	5.3
+ 0.1 M CsCl	25.7 ± 8	0.11	0.65	10
+ 0.1 M $MgCl_2$	30.0 ± 5	0.15	0.90	12

After calibration of the photochemical system using ferrioxalate actinometry, quantum yields were determined for the early linear region of methanol production (0-2 hr). Quantum yields for methanol rise from 4.6 x 10^{-6} to 1.4 x 10^{-4} with the optimization of Ru:py ratios and added potassium electrolyte. The larger quantum yields are comparable with those reported for the photochemical reduction of CO_2 to CH_4 catalyzed by the combination of $[Ru(bpy)_3]^{2+}$ and noble metal colloids (ϕ = 1x 10^{-4})[148] and only slightly less than that reported for the photochemical reduction of CO_2 to CO as catalyzed by $[Ru(bpy)_3]^{2+}$ with Ni-cyclams (ϕ = 1x 10^{-3}).[105,107] In all these comparisons, quantum yields are reported in moles of electrons produced per mol photons absorbed.

While methanol was the desired product, formate was the dominant reduction product. TON ranged from 1 to 76 depending on conditions which give quantum yields for formate production as high as 0.02 (see Table 2.1). These quantum yields are on par with those of various intermolecular systems for formate production which range from 0.01 to 0.09 and reaching as high as 0.15.[149] As seen from Table 2.1, formate yields improve at low pyridine to Ru ratios, in contrast to the methanol trend, however the most significant component for formate production appears to be the presence of the KCl. Addition of this component to the 200 py: 1 Ru photolysis solution increased TON from 9

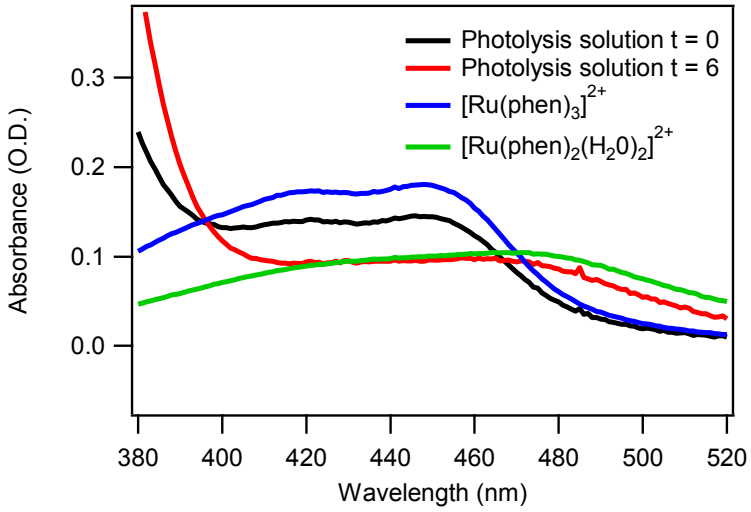

Figure 2.3 Absorption spectra of: $[Ru(phen)_3]^{2+}$ the photolysis solution and suspected complexes. In the graph above is chromophore $[Ru(phen)_3]^{2+}$ in water, the blue line, and the photolysis solutions with no irradiation have similar absorption spectra between 380 nm and 500 nm, black line indicating the same species in solution. However, after 6 hours of irradiation, red line, the absorption of the solution starts to resemble that of $[Ru(phen)_2(H_2O)_2]^{2+}$, green line, which suggests the formation of the diaquo species in solution

to 76 formates per Ru; the largest increase seen. While the effect of added K^+ is not completely understood, it appears that ion-pairing stabilization of the carbamate radical or carbamate greatly improves the reaction yield. It is notable that the build-up of formic acid in our system is in agreement with Borcarsly and coworkers findings that formic acid

reduction is the RDS for the pyridine-catalyzed CO_2 reduction to methanol.[119] Optimization of this system for formate production was beyond the scope of this work and is planned in upcoming studies.

At present, the productivity of this system is limited by the stability of the chromophore. Photolabilization of the diimine ligand in $[Ru(phen)_3]^{2+*}$ and $[Ru(bpy)_3]^{2+*}$ systems has been reported as the most common decomposition pathway[150] and this process is usually exacerbated in aqueous solution. Examination of the visible spectrum of the solution shows significant changes in the chromophore spectrum consistent with ligand labilization (Figure 2.3) and these decomposition products, such as $[Ru(phen)_2(H_2O)_2]^{2+}$, are photochemically inactive.

While all the details of the CO_2 reduction mechanism are still unknown, reduction of the pyridinium ion by the ruthenium chromophore to the neutral pyridinium radical is thought to be an essential initial step. Figure 2.4 depicts two distinct pathways, A and B, which could give rise to the pyridinium radical. In A, the pyridinium ion acts as a quenching agent for excited Ru complex, the yielding the pyridinium radical and $[Ru(phen)_3]^{3+}$, a strong oxidizing agent, which is subsequently reduced by the ascorbate. In B, ascorbate reduces the to yield a strong reducing agent, $[Ru(phen)_2(phen^{-\cdot})]^{+}$ which is capable of reducing the pyridinium ion. If we use the more negative of the reduction potentials listed for the pyridinium ion (E_{red} ($PyH^+/PyH^{\cdot}$) = -0.95 V with a dropping Hg electrode and -0.34 V with a Pt electrode), only pathway B is possible as the pyridinium ion is incapable of oxidatively quenching the Ru complex excited state in A. If the lower pyridinium reduction potential is realized in homogeneous solution (without the electrode) both pathways are possible. In general pathway B is preferred, as the large concentration and negative charge of the ascorbate both favor reductive quenching with $[Ru(phen)_3]^{2+*}$ to generate the strong reducing agent $[Ru(phen)_2(phen^{-\cdot})]^{+}$. We postulate

that once this species is generated, formation of the pyridinium radical follows and the subsequent steps for CO_2 insertion and reduction to methanol are equivalent to those postulated by Bocarsley and coworkers.

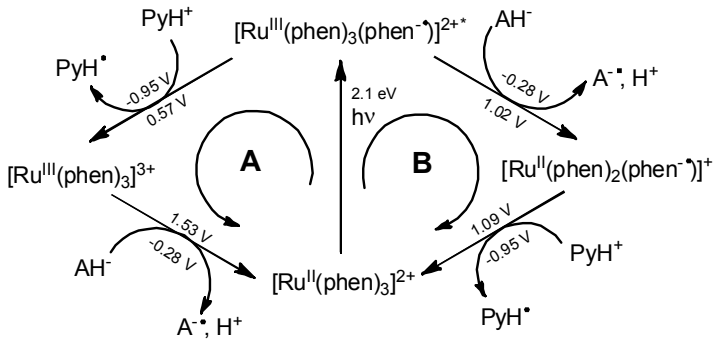

$$AH^- + PyH^+ \longrightarrow A^{-\bullet} + H^+ + PyH^\bullet \quad +1.23\ eV \quad (1)$$

Figure 2.4 Oxidative and reductive quenching pathways for electron transfer and photocatalytic driving of reaction 1. PyH^+ = pyridinium and AH^- = ascorbate.

Our results show that metal surfaces are not a requirement for pyridine-catalyzed deep CO_2 reduction. However, this does not necessarily mean that they could not participate or even enhance these processes. The exact role of the surface in the electrochemical systems is a matter of debate with various theoretical studies suggesting the Pt and Pd surfaces are necessary for the formation of surface-hydrides,[151] or that pyridinium radicals are incapable of reducing CO_2 in homogeneous solution at such low overpotentials.[141] This latter study has been countered by other theoretical work showing the pyridinium radical to be competent for CO_2 reduction.[152] It is also possible that the positive shift in the reduction potential on these particular electrodes is unrelated to the CO_2 reduction mechanism other than to lessen the extent of other side reactions which occur at more negative potentials. To examine this, we added 0.08 mg/ mL of metallic Pt, Pd, Ni, or Au (45-50% by mass) on carbon black as heterogeneous co-catalysts or

~0.01 mg / mL quantity of colloidal Pt solution to the typical 200:1 pyridine: ruthenium mixture (total volume 25 mL). As shown in the data in

			MeOH			Formate		
Ru:py	n	pH	μMa	TON MeOHa (in e-)	Φc 10-5	mM b	TON Formate (in e-)[b]	Φc 10-3
2:1	1	5.0	0.00 ± 1	0.0	0.0	4.7	19 (39)	1
1:1	1	5.0	6.3 ± 2	0.03 (0.19)	0.75	2.6	11 (22)	0.6
1:2	1	5.0	6.1 ± 1	0.03 (0.18)	0.46	0.42	1.8 (3.6)	0.1
1:100	1	5.0	29 ± 3	0.14 (0.87)	2.6	0.26	1.0 (2.0)	0.06
1:200	3	5.0	31 ± 3	0.15 (0.92)	6.3	2.2	9 (18)	3
1:200 (0.1 M KCl)	3	5.0	66 ± 12	0.33 (2.0)	11	18	76 (152)	25
1:200 (pH 4.0)	2	4.0	0.00 ± 2	0.0	0.0	2.9	12 (24)	4
1:200 (pH 6.0)	2	6.0	13 ± 0.3	0.05 (0.31)	2.7	1.1	4.5 (9.0)	0.9

Conditions: pH 5.0, 0.20 mM $[Ru(phen)_3]^{2+}$, 0.1 M ascorbic acid, CO2, py redistilled. [a] After 6 h irradiation, methanol as a function of ruthenium with electrons as a function of ruthenium in parentheses. [bAfter] 1 h irradiation, formate as a function of ruthenium with electrons as a function of ruthenium in parentheses. [c] □ reported on a per electron basis as a function of the slope of the initial linear portion of the product vs time plot.

Table 2.2, addition of Pt and Pd metal co-catalysts lowered methanol yield by ~15% whereas Ni on carbon and Au on carbon cut yields by 50%. Addition of colloidal Pt shut down methanol production completely. Thus, the role of these surfaces in the electrochemical process is still unclear but it is obvious that they are not a requirement for the pyridine-based CO_2 reduction process.

2.3 Conclusion

In summary, the photochemical reduction of carbon dioxide to formate and methanol has been observed in an aqueous system containing a chromophore, ascorbic acid, and pyridine. While the dominant product is the two-electron-reduced formate, to the best of our knowledge, this is the first homogeneous photochemical system capable of direct reduction of CO_2 to methanol and clearly demonstrates the ability of pyridine, in the presence of a suitable chromophore, to catalyze the deep reduction of CO_2 to methanol without a metal surface. The presence of group 1 metal cations in solution aids the reduction of carbon dioxide to methanol and formate possibly by stabilizing the py-CO_2 adduct that forms through ion-pairing with the oxygen of one or more of the intermediate species formed during the reduction process. In the presence of potassium ion, the 8-fold increase in formate production is mirrored by a 2-fold increase in methanol yield supporting the supposition that formate (or formic acid) undergoes subsequent pyridinium-based reduction to methanol.[119] However, a more detailed analysis of this latter step is now warranted to firmly demonstrate that this “intermediate” is further reduced to methanol. We are continuing our studies of this system with the goals of improving chromophore stability, improving selectivity for methanol, and replacing the sacrificial donor with more practical donors.

2.4 Experimental

2.4.1 Chemicals

Solvents used were used as received unless otherwise noted. Water used was from a Millipore purification system. Pyridine was purchased from Sigma Aldrich and was distilled before use. The ruthenium(III) chloride tris-hydrate was purchased from Pressure chemical and used as received. The 1,10-phenathroline and ammonium hexafluorophosphate were purchased from Alpha Aesar both chemicals were used as received. Ascorbic Acid was purchased from Alpha Aesar and was washed by dissolving in water and evaporating the water off using a rotating evaporator six times.

$[Ru(phen)_3]Cl_2$ was prepared in a similar manner as reported in the literature.[153] NMR matched that reported in literature for this complex. ^{1}H NMR: (400 MHz MeCN-d3) δ 7.99 (dd, 6H); 8.22 (s, 6H); 8.56 (dd, 6H). The hexafluorophosphate salt of the complex was converted back to a chloride salt, by dissolving the salt in acetone and adding excess tetrabutyl ammonium chloride in acetone, the resulting precipitate was filtered and washed three times with 15 mL acetone.

2.4.2 Photolysis

The photoreactor, Figure 2.5, used for photolysis reactions was constructed using one hundred twenty, 470 nm LEDs that are 5 mm in diameter. They were connected in 24 parallel circuits consisting of 5 LEDs/circuit. Glassware for photoreactor was custom built and was constructed of borosilicate glass with > 90 % transmittance in the window of 330 nm to 1000 nm. The inner reaction compartment had a diameter of 20 mm and a total volume of 30 mL. This compartment was surrounded by a borosilicate water jacket (one piece construction) with inlet and outlet adaptors, so that the temperature could be held constant. The OD of the entire cell was 48 mm and fit snugly into the photodiode lamp holder. The reactor could be sealed with standard 24/40 rubber

septa which allowed the introduction of CO_2 via a needle and, if needed, an optical UV-vis probe. Chemical actinometry using potassium ferrioxalate[154] gave an average photon flux of 36 x 10^{-3} Einstein h^{-1}.

Figure 2.5 Photoreactor as used in photolysis experiments for photoreduction of carbon dioxide.

All photolysis reactions were performed following the same general procedure. To a 25.0 mL solution of water containing 0.88 g ascorbic acid and 100.0 µl pyridine adjusted to pH 5 with 10 M NaOH, 4.0 mg $Ru(phen)_3Cl_2$ is added. The resulting solution is degased with nitrogen for 30 minutes and saturated with carbon dioxide for 30 minutes. A sample is taken before the photoreactor is turned on and again every hour for 6 hours and are frozen immediately after collection at -20 C.

2.4.3 Analysis of Products

The samples from this experiment were desalted by a trap to trap distillation procedure which could quantitatively transfer the water, methanol, and acetonitrile (internal standard) in the samples. Desalted samples were subjected to GC-MS using a QP2010 SE GC-MS, equipped with an AOC-20i automatic sample injector (Shimadzu Scientific Instruments Inc., Columbia, MD, USA). The GC was equipped with a SHRXI-

5MS fused silica capillary column (30m, 0.25 mm i.d., 0.25 μm film thickness) and run using helium as a carrier gas with a flow rate of 1.0 mL/min, a column inlet pressure of 51.5 kPa and injections were made with a split ratio of 20:1. Inlet and detector temperature was set at 250°C and the oven temperature was maintained isothermally at 40°. The methanol quantification was achieved by using acetonitrile as the internal standard and calibration curves obtained from known samples treated identically. Single ion mode (SIM) was typically used with m/z 31 and m/z 41 monitored as quantification ions for methanol and acetonitrile respectively.

Samples for NMR were prepared by treatment with 0.3 mL of 10 M NaOH and evaporated to dryness. This residue was dissolved with 0.6 mL D_2O with 100 uM of DSS (DSS = Sodium 4,4-dimethyl-4-silapentane-1-sulfonate). The following peaks were used to roughly quantify the formate, δ 8.63 ppm (1H, HCOO) the formate peak and δ 0.0 (9H, CH_3) from the DSS. The concentration of formate was calculated based on a calibration curve and also from the ratio of the two peak compared with the concentration of the DSS. Numbers both way came out to the same number.

Chapter 3

ELECTROCATALYTIC AND PHOTOCATALYTIC REDUCTION OF CO_2 USING RUTHENIUM COMPLEXES CONTAINING PYRIDYL GROUPS

3.1 Introduction

The reactivity of CO_2 towards coordinatively unsaturated transition metal complexes under modest (near ambient) conditions have been studied for many years,[155] because of concerns about the effect of CO_2 on the environment and the contribution that carbon based fuels may have; has led to a resurgence in research in this area. (i.e. CO, formate) confirming the early promise of using transition metal complexes as catalysts for this type of transformation.[156] Some of the early studies include the report by Meyer and coworkers stating that Rh and Ir polypyridyl complexes are competent electrocatalysts for CO_2 reduction to formate in DMF under air-free, ambient conditions.[64] Since then, there have been significant contributions in both electrocatalytic and photocatalytic CO_2 reduction studies by a number of groups including Meyer,[28,85,86,127-129,157] Fujita,[17,18,131,158,159] Kubiak,[11,160] Saveant,[156] Abruna,[47,161-163] Bocarsly,[1,2,9,73,74] and Crabtree[164] among others.[99,132,138,165]

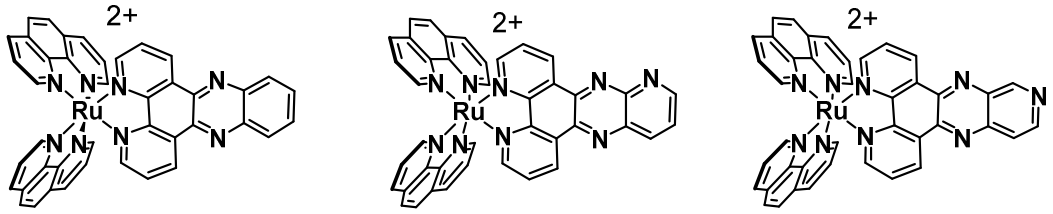

$[(phen)_2Ru(dppz)]^{2+}$ **Rudppz** $[(phen)_2Ru(ptpb\alpha)]^{2+}$ **Ruα** $[(phen)_2Ru(ptpb\beta)]^{2+}$ **Ruβ**

Figure 3.1 Structures of $[(phen)_2Ru(ptpb\alpha)]^{2+}$ and $[(phen)_2Ru(ptpb\beta)]^{2+}$ complexes and their precursor $[(phen)_2Ru(dppz)]^{2+}$ complex.

Of these various approaches towards catalytic CO_2 reduction, the work of Bocarsly et al. stands out for its use of a simple organic compound as a catalyst, pyridine, which they reported is capable of producing the 6 electron reduced product over the 2 electron reduce product, which is produced by far more CO_2 reduction systems.[1,2] The advantage of this over other systems for CO_2 reduction is the direct production of a transportation fuel. It is theorized that this six-electron process occurs in a sequentially manner starting with the reduction of the pyridinium cation (pyH^+) to the neutral radical ($pyH^\bullet$) which is followed by insertion of CO_2 into the NH bond to give a radical carbamate intermediate. Subsequent sequential reductions lead to the final product of methanol.

Work in Chapter 2 demonstrated this process could be done photochemically in homogeneous aqueous solution using $[Ru(phen)_3]^{2+}$ as the chromophore, pyridine as the CO_2 reducing catalyst, and ascorbic acid as the sacrificial donor.[166] While this photochemical process has poor selectivity for methanol production, strongly favoring formate, it did demonstrate that the pyridinium-based catalysts can reduce CO_2 to methanol in the absence of a metal surface, which had previously been described as essential in some recent theoretical works.[75,141] The success of this bimolecular system, although limited, encouraged further study in this area. By switching to a unimolecular photocatalyst which would incorporate both the ruthenium chromophore and the pyridine CO_2 reducing co-catalyst would simplify electron-transfer process to a simple intramolecular process. Such a system would, in theory, eliminate the need for a large excess of pyridine relative to Ru chromophore and speed up the CO_2 reduction process.

In this chapter, the performance of Ruα and Ruβ as electrocatalysts and photocatalysts for multiple electron reductive process on CO_2 is reported. Using a combination of voltammetry and differential reflectance measurements, we elaborate on the photochemical and electrochemical reduction mechanism and complexes speciation

in the absence and presence of CO_2. Constant-current electrolyses and constant irradiation photolysis along with gas chromatography determined methanol to be one of the CO_2 reduction products.

3.2 Results and Discussion

3.2.1 Approach for Photo- and Electrocatalytic CO_2 Reduction by Ruα and Ruβ

Relevant photochemical and electrochemical data for Rudppz, Ruα, and Ruβ are collected in Table 3.1. All three are weak or non-emitting in aqueous solution, but exhibit

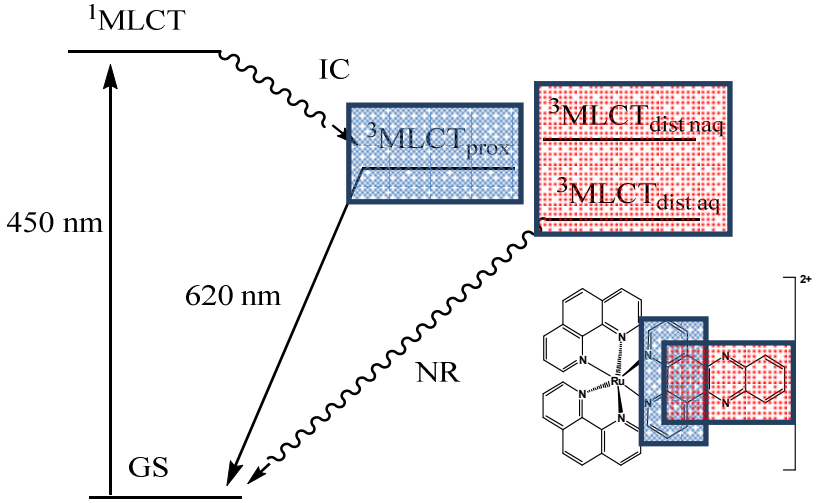

Figure 3.2 Jablanski diagram of Rudppz where the proximal state and distal states are shown in blue and red respectively. The distal state is shown with 2 levels that are relative to the proximal state and solvent dependent. In non-aqueous environments the distal state is higher in energy and not readily accessible, in aqueous environments the distal state is much lower in energy and lead to non-radiative decay.

strong (or bright) emission in non-aqueous solvents such as MeCN. Turro and Murphy have shown that mixed-aqueous solutions also exhibit enhanced luminescence lifetimes; for example, Rudppz has a luminescent lifetime of ca. 400 ns in 1 M H_2O in DMF compared to 250 ps in pure water.[167,168]

The sensitivity of the luminescence lifetimes in these complexes is attributed to the presence of two energetically similar triplet states, $^3MLCT_{prox}$ and $^3MLCT_{dist}$, which

formally localize the excited electron in a proximal[169] 'bpy-like' MO on the extended ligand or in a distal 'phenazine-like' MO, respectively, inset in Figure 3.2. In aqueous solution, Rudppz emission is weak and red shifted (~ 670 nm, ϕ_{lum} = 2.5 x 10^{-6}) relative to that in MeCN (610 nm, ϕ_{lum} = 0.033)[169] due to population of the $^3MLCT_{dist}$ state being favored in water and the $^3MLCT_{prox}$ state being favored in MeCN, see Figure 3.2. As the proportion of water is increased in the mixed solvent system the lifetime of the excited state drops which reflects a shift in the excited-state equilibration between the two states from favoring the $^3MLCT_{prox}$ state to the $^3MLCT_{dist}$ state.[170-172] As Ruα and Ruβ exhibit largely analogous luminescent behavior, it is thought that they have similarly behaving $^3MLCT_{prox}$ and $^3MLCT_{dist}$ excited-states.

Table 3.1 Absorption maxima, emission maxima, quantum yields, first reduction potentials, and pK_a values for complexes Rudppz, Ruα, and Ruβ. pKa's for Ruβ and Ruα were found experimentally.

		MeCN			H_2O					
Complex	λ_{ex} nm	λ_{em} nm	ϕ_{lum} (10^{-3})	τ ns	λ_{em} nm	ϕ_{lum} (10^{-5})	τ ps	$E_{1/2}$ V	pK_a	ref
Rudppz	445	610	33	663	670	2.5	250	-0.81	-1	169,172, 173
Ruα	440	609	< 5	460	745			-0.64	< 0	172,174, 175
Ruβ	442	613		460				-0.57	2.0	174,176

3.2.2 Electrochemistry of Ruα and Ruβ in N_2- and CO_2-Saturated Solutions

The first redox process for Ruα and Ruβ in N_2 saturated DMF:H_2O (1M) shows highly reversible voltammetric waves (v = 50 mV/s) at redox potentials, E^0, of -0.64 V and -0.57 V vs Ag/AgCl respectively (Figure 3.3a). These reductions are assigned to reduction of the ptpbα and ptpbβ ligands. These redox processes were found at slightly

more positive potentials than that observed for Rudppz (located at -0.81 V vs. Ag/AgCl) in dry DMF and at -0.80 V after addition of water.[177] The positive shift in potentials for Ruα and Ruβ is reasonable given the extra nitrogen that is part of these ligands relative to dppz leading to an increase the overall electronegativity of the ligand. Figure 3.3b shows the effect of concentration of complex Ruα on cyclic voltammograms (CVs) spanning the first electroreduction of the complex. As the concentration was varied from 0.5 to 3.0 mM, the shape of the voltammograms and the peak separation afforded Nernstian

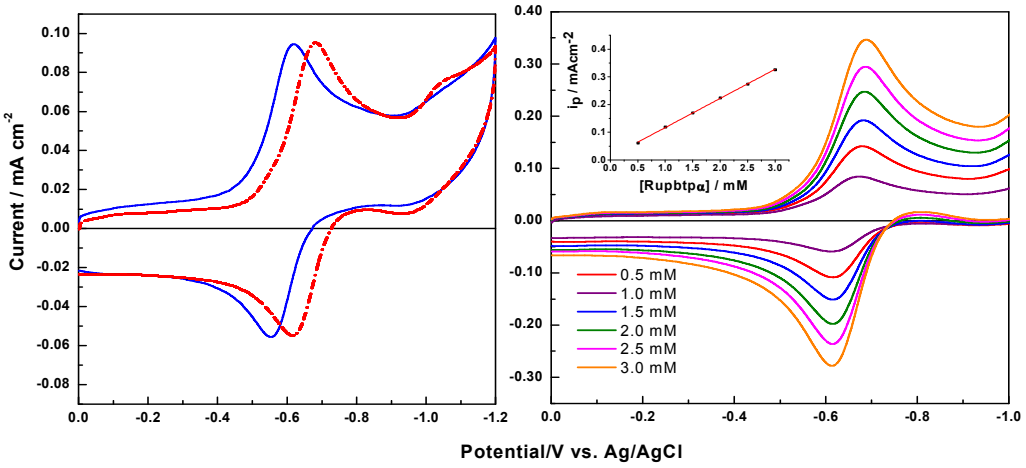

Figure 3.3 (a) Comparison of the voltammetric behavior of Ruα (red dash line) and Ruβ (blue solid line) in N_2 saturated DMF/H_2O (1 M) solutions. Working electrode: Glassy carbon disk (1mm dia.), scan rate = 50 mV/s, complex concentration = 20 μM, supporting electrolyte = 0.1 M TBAPF6. (b) Effect of concentration on the voltammetric behavior of the first electroreduction process of Ruα in solutions saturated with N_2. The increase of the cathodic current peak with the complex concentration follows a linear relationship (shown in the inset plot).

(reversible) behavior under diffusion control for this complex in the absence of CO_2. From the linear slope of the cathodic current peak vs complex concentration plot (inset to Figure 3.3b), it was determined that it is a one-electron process, assuming a diffusion coefficient of 3 x 10^{-6} cm^2/s.[178] A Pourbaix analysis in water of the three complexes showed that the pKa's of the conjugate acids for Rudppz, Ruα to be less than 0 and 2.0

for Ruβ. Both Ruα and Ruβ show pH dependence redox potentials at pHs > pKa consistent with a 1 proton 1 electron process up to pH 7.

The electrocatalytic reduction of CO_2 is by Ruα and Ruβ, is observed by simply bubbling CO_2 through the DMF:H_2O solution and examining the CVs, particularly when performed at low potential scans rates (5-10 mV/s). As seen in Figure 3.4, large increases in the cathodic current are observed at -0.64 V and -060 V for solution of Ruα

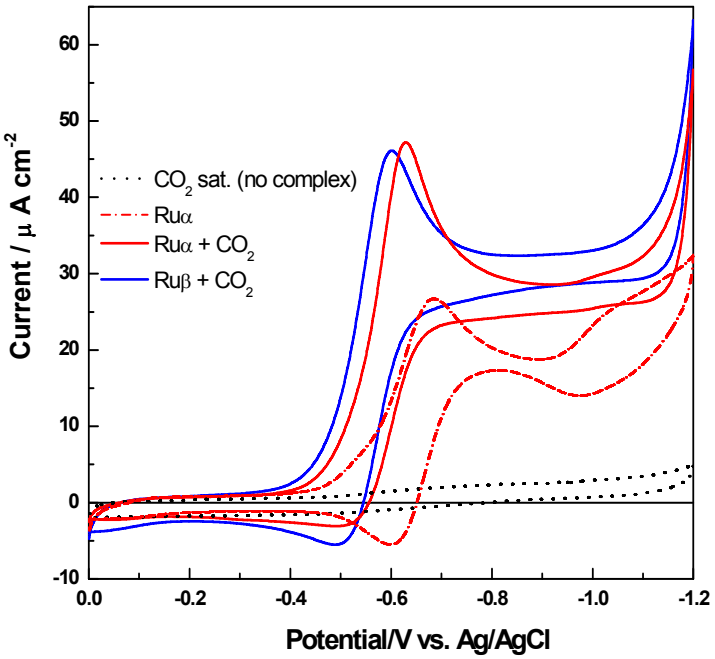

Figure 3.4 Comparison of the voltammetric behavior of **Ruα** (red solid line) and **Ruβ** (blue solid line) in DMF/H_2O (1 M) solutions saturated with CO_2. Voltammograms of **Ruα** before saturation with CO_2 (red dash line) and that without Ru complex but with CO_2 (black dot line) are included as reference. All voltammograms were run at 5 mV/s with a glassy carbon working electrode.

and Ruβ, respectively, indicating electrocatalytic CO_2 reduction. Rudppz, in contrast, is not electrocatalytically active when under identical conditions when CO_2 is added (data not shown), indicating the need for the extra nitrogen in the ligand structure for catalytic activity. A control run of CO_2-saturated solution without addition of any of the ruthenium

complexes (Figure 3.4, black dot trace) indicates that glassy carbon is not active for CO_2 reduction. In the absence of a catalyst and in media of low proton availability (such as DMF and DMSO) electroreduction of CO_2 is reported to occur at -2.16 V vs. Ag/AgCl.[114]

The voltammetric behavior of both complexes in CO_2-saturated solutions is similar in shape although Ruβ shows a cathodic peak at less negative potentials than its Ruα analog indicating a more facile interaction with CO_2 for the first complex. In both cases, the presence of a reactive nitrogen site on the ptpb (either α or β) ligand facilitates the formation of a CO_2 adduct, presumably in the form of a carbamate-type intermediate.[1] Figure 3.4 shows a net increase of cathodic current at potentials more negative than -1.1 V for both complexes, indicating that the reduction CO_2 is also catalytically occurring at these potentials (absence of the complex shown as the dot line). This is important in the view of the photochemical reduction of CO_2 as the ^{1}MLCT excitation of the Ru dπ→ ptpb π band in any of the complexes and reductive quenching of the ^{3}MLCT excited state by TEA could trap the electron on the ligand ptpb to form $[(phen)_2Ru^{II}(pbtp\beta^{\bullet -})]^+$ either in the bpy structure of the ptpb or at the farther nitrogen of the structure.

The second reductive redox process seen for Ruα (Figure 3.4e) at -1.05 V disappears when CO_2 is present and that the wave is absent in the CV for Ruβ (Figure 3.3a). It is notable that the magnitude of this follow-up wave increases at lower scan rates (compare the CVs in Figure 3.3a (50 mV/s) and Figure 3.4 (5 mV/s)). This behavior suggests that the radical $[(phen)_2Ru^{II}(ptpb\alpha^{\bullet -})]^+$ is undergoing dimerization in the absence of a substrate and that the new dimer is the resulting electroactive species. The small change in location of the most distal nitrogen for Ruβ is apparently enough to inhibit this side reaction, suggesting that the most distal carbons are the site of dimerization.

3.2.3 Product Yields in the Electrocatalytic CO_2 Reduction

In order to determine the extent of CO_2 reduction, 300 μM of Ruβ was subjected to controlled-current electrolysis in CO_2-saturated a DMF:H_2O solution, the potential profile of which is shown in Figure 3.5a. The electrode potential is seen to stabilize at ca. -0.6 V (first electroreduction process of the complex) for a period of time spanning 6 h. After this the potential is seen to rapidly evolve to more negative values associated to the second electroreduction of the complex and remains there for at least 15 hours. The abrupt negative potential shift at ca. 6 h of electrolysis, signals the end of the first

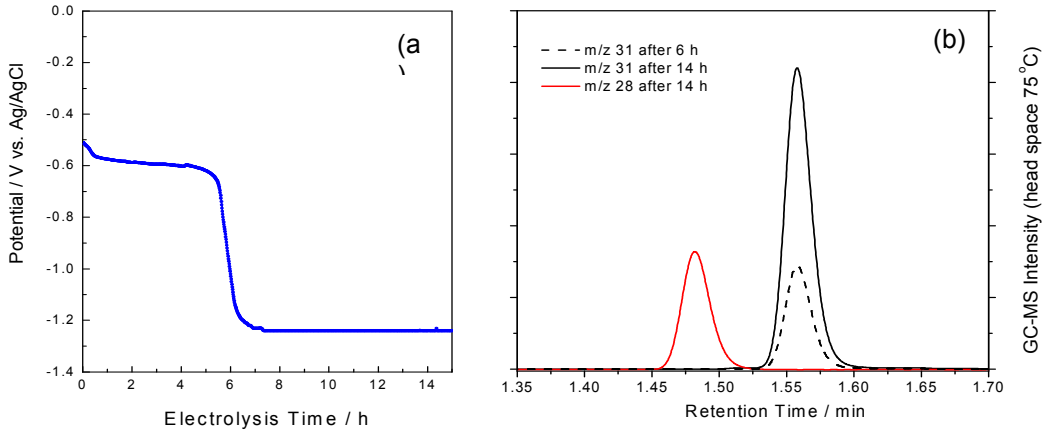

Figure 3.5 (a) Potential/time profile recorded during cathodic galvanostatic electrolysis of **Ruβ** (300 μM) in DMF: H_2O (1M, pH 5.5) saturated with CO_2. (b) Head space GC-MS analyses of liquid aliquots removed after 6 and 14 h of electrolysis respectively. MS peak intensities at 1.56 min (m/z = 31) from CH_3OH increase ca. 2.5 times from 6 to 14 h of electrolysis. Formation of CO (m/z = 28, at 1.47 min, red trace) is only present after the potential has evolved to ca. -1.2 V. Electrolysis conditions: 0.1 M $TBAPF_6$ (0.1 M) as supporting electrolyte; working electrode = RVC cylindrical electrode; applied current = -0.6 mA.

electrocatalytic process. A coulometric calculation of the number of electrons consumed in the time period of the first plateau reveals that 5.5 equivalents of electrons per Ruβ were consumed during this electrolysis period (at -0.6 V). Aliquots removed during the electrolysis were heated to 80 °C and subjected to headspace GC-MS analysis to determine if volatile products like methanol or carbon monoxide were produced. After 4

to 6 hours of electrolysis, GC-MS data revealed that methanol was being produced during the initial electrocatalytic period when the potential was~ -0.6 V. MS detection was performed at m/z values of 31 (CH_2OH^+) and 28 (CO^+) to track formation of CH_3OH and CO respectively. Data from a typical run after 6 hours and 14 hours electrolysis are shown in Figure 3.5b. In both timeframes, the main product formed was methanol which is uniquely tracked by the m/z = 31 signal. Formaldehyde, detected at m/z 29, was the second predominant product at 6 hours electrolysis. After 14 hours of electrolysis, methanol build up is more than double that found at 6 hours (Figure 3.5b). The product distribution changes after the potential changes to ca. -1.2 V. While the main product is still methanol, at ~ 900 μM, the second dominant product was CO which is only produced at these more negative potentials. It is apparent that Ruβ still catalyzes CO_2 reduction at the more negative potentials with product distribution being 75% of methanol 25 % CO after 14 hours of electrolysis. A TON of approximately 1 for the formation of methanol at 6 h and 3 at 14 h was obtained with respect to the complex used. Detection of formaldehyde by the chromotropic acid test corroborated the GC-MS data for formaldehyde. This qualitative tests were performed after removal of the electrolyte and ruthenium complex using an Amberlite IRN-150 ion-exchange resin because the Ru complex interfered with the colorimetric test.

3.2.4 Effect of CO_2 on the Photochemistry of Ruα and Ruβ Complexes

In order to assess the capability of Ruα and Ruβ as visible light photocatalysts for CO_2 reduction, the UV-visible absorption spectrum was examined. The absolute spectra of Ruα(Figure 3.6a) and Ruβ (Figure 3.6b) in a CO_2-saturated solution containing 0.25 M TEA before and after visible light irradiation. This figure also contains the difference absorption spectra, ΔA, for each complex in order to show more clearly the spectral

changes. The evolution of the ΔA as a function of irradiation time for Ruα and Ruβ (Figure 3.7) is in degased (Figure 3.7a and Figure 3.7c) and CO_2 saturated (Figure 3.7b

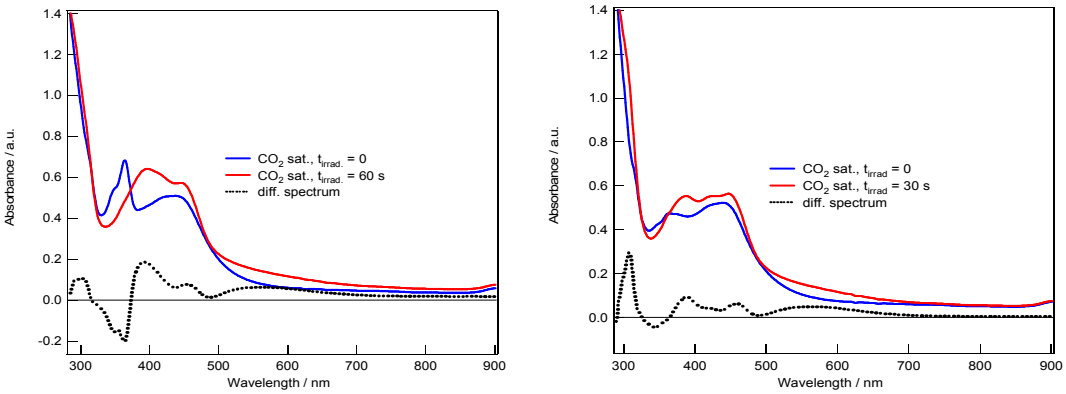

Figure 3.6 Comparison of the photochemical changes of **Ruα** (a) and **Ruβ** (b) in a CO_2 saturated DMF:H_2O solution: spectra before irradiation (blue solid line) and after irradiation (red solid line). Spectra in black dots correspond to the spectral difference, ΔA, between irradiated and dark conditions for **Ruα** (a) and **Ruβ** (b) respectively. Complex concentration is 22 μM in both cases and [TEA] = 0.25 M.

and Figure 3.7d) DMF:H_2O solutions respectively. Both complexes show similar, but not identical behavior under either N_2 or CO_2 atmospheres with a rapid bleaching of the ptpba or ptpbb LC bands around 360-380 nm. These spectral changes are consistent with reductive quenching of the Ruα* or Ruβ* excited-state complexes by TEA to yield the one-electron reduced products $[(phen)_2Ru^{II}(pbtp\alpha H^{\bullet})]^{2+}$ ($Ru\alpha H^{\bullet}$) and $[(phen)_2Ru^{II}(pbtp\beta H^{\bullet})]^{2+}$($Ru\beta H^{\bullet}$). This LC bleach is particularly noticeable in the Ruα spectra. For Ruβ the growth of two sharp bands at ca. 390 and 460 nm and one broad absorbance at 575 nm is apparent in both N_2 and CO_2 atmospheres suggesting that addition of CO_2 to the photoreduced $Ru\beta H^{\bullet}$ is not fast or does not significantly change the absorption spectrum relative to the protonated complex. Even though spectral changes are not evident, the time needed to reach a steady-state spectral profile is ~ 2.5 times faster in the presence of CO_2. The similarity of the Ruα final spectrum after

photolysis under CO_2 suggests the same is true for RuαH$^{\bullet}$, either it's slow to add CO_2 or addition does not noticeably perturb the spectrum relative to protonated radical.

Figure 3.7a and b compares the photochemistry of Ruβ (2.2×10^{-4} M) under continuous irradiation in degased (Figure 3.7c) and CO_2 saturated (Figure 3.7d) solutions containing TEA. In contrast with the effect of CO_2 in the photochemical spectral evolution of Ruα, the respective ΔA spectra of Ruβ showed very similar spectral features with and without CO_2. The main changes observed are the bleaching of the 344-nm peak (as characteristic of the initial complex concentration) counterbalanced with the growing of bands at 308, 388, 458 and 564 nm. The time to reach the steady-state spectral profile is slightly shorter in the presence of CO_2 (vide infra, Figure 3.7) getting there in 30 s vs. ca. 75 s in degased media, i.e. ~ 2.5 times faster. These changes are consistent with a one-electron reduction of the complex, induced by the $MLCT_1$ excitation of the Ru dπ → ptpbβ π transition followed by reductive quenching of the ^{3}MLCT state by TEA to trap the electron on the ptpbβ ligand to form $[(phen)_2Ru^{II}(ptpb\beta^{\bullet -})]^+$. This reduced complex is stable and can be re-oxidized to the starting complex $[(bpy)_2Ru(ptpb\beta)]^{2+}$ upon introduction of air.

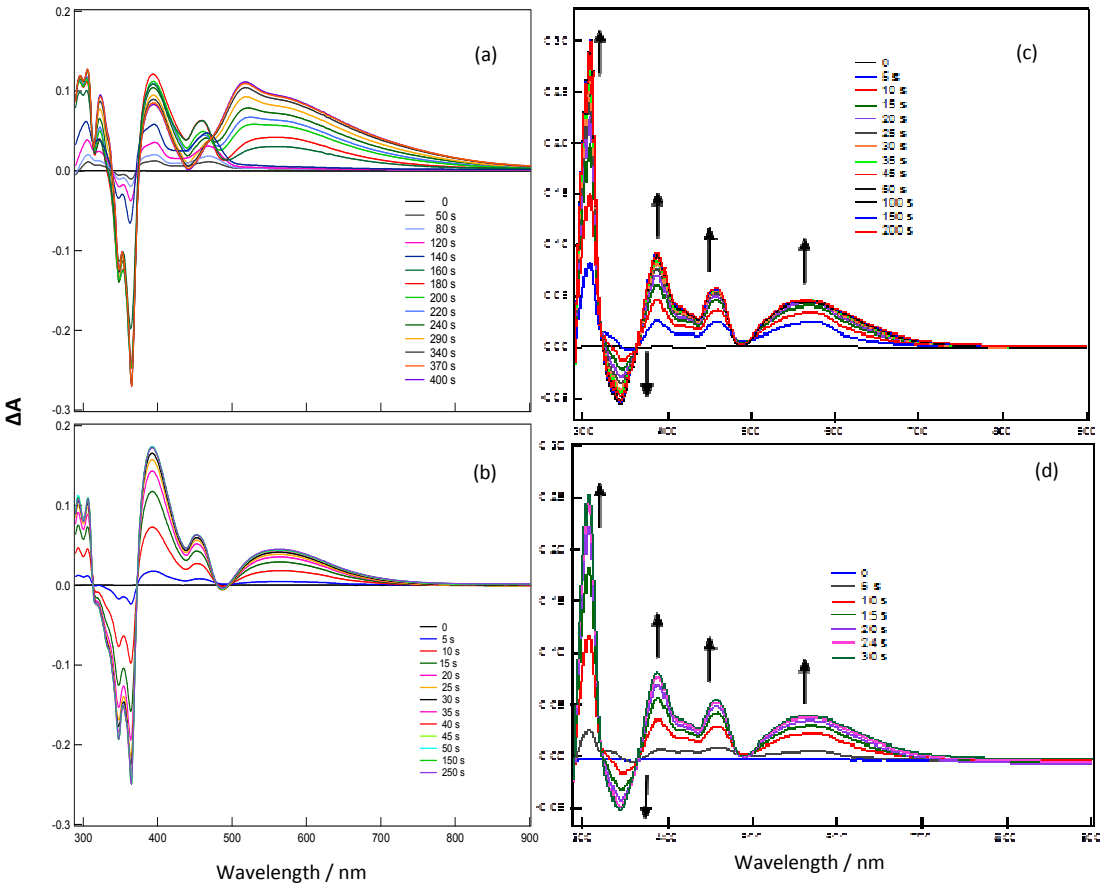

Figure 3.7 Transient ΔA spectra of Ruα (2.2 x 10-4 M) during photolysis in N_2 (a) and in CO_2 (b) saturated DMF/TEA (0.25 M)/H_2O (1 M) solutions and Ruβ (2.2 x 10-4 M) during photolysis in Ar (c) and in CO_2 (d) saturated DMF/TEA (0.25 M)/H_2O (1 M) solutions. Peaks pointing down indicate bands disappearing while those pointing up correspond to new bands appearing due to photolysis.

Serial experiments of cycles of 30 s irradiation / 5 min dark periods (for CO_2 replenishing in the photochemical cell) were carried out, shown in Figure 3.8. Ruβ (2.2 x 10^{-4} M) was used under 30 s continuous irradiation in CO_2 saturated solutions containing 0.25 M TEA as sacrificial donor. The irradiation time was chosen to detect steady-state level of species absorbing at the 564 nm and 344 nm bands respectively. During the irradiation times, the band at 564 nm senses the formation of the protonated monoreduced ($Ru\beta^{\bullet-}$ → $HRu\beta$) species in DMF:H_2O, while the band at 344 nm is just

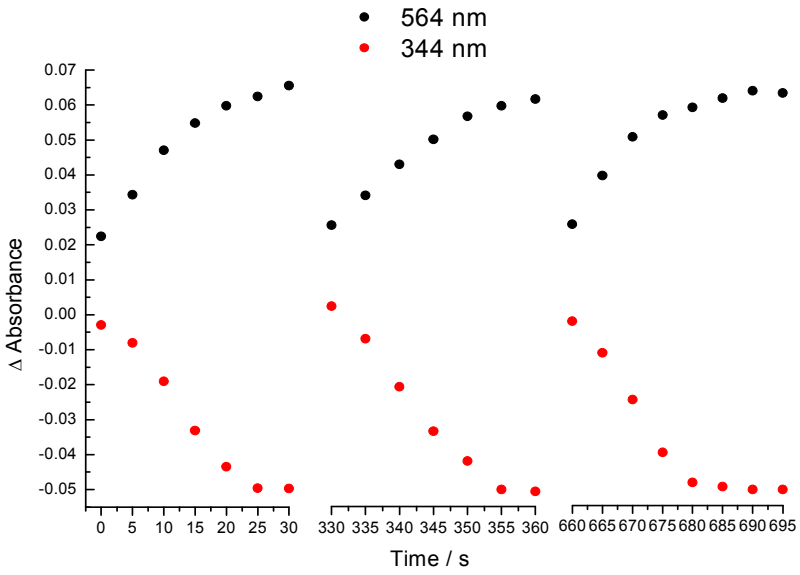

Figure 3.8 Three consecutive photocatalytic periods of **Ruβ** (2.2 x 10^{-4} M) in CO_2 saturated DMF/H_2O (1 M)/TEA (0.25 M) solutions. The photoreduced complex is manifested by the growth of a band at 564 nm at expense of the 344 nm band characteristic of the unreduced photocatalyst. Each photoreduction process required 30 s to be completed and it was separated from the next cycle by a 5 min CO_2 bubbling in the dark. The period of CO_2 bubbling gives rise to the removal of the reduced CO_2 species coordinated to the complex and thus releases the complex to work again in the next irradiated period.

indicating the disappearance of the initial Ruβ complex. The three irradiated periods

showed very similar temporal profiles for both HRuβ and Ruβ species pointing to reversible photocatalyst regeneration.

Table 3.2 A comparison of the photosystem from Chapter 2 and Ruβ system

	MeOH			Formaldhyde			Formate		
	μM	TON (in e^-)	Φ 10^{-5}	μM	TON (in e^-)	Φ 10^{-3}	mM[b]	TON (in e^-)	Φ 10^{-3}
Ruβ DMF:water	45	0.4 (2.6)	15	285	2.9 (5.8)	1.6	0.65	6.5 (13)	3.6
1:200 $Ru(phen)_3$:py water	31 ± 3	0.15 (0.92)	6.3	-	-	-	2.2	9 (18)	3
1:200 $Ru(phen)_3$:py (0.1 M KCl) water	66 ± 12	0.33 (2.0)	11	-	-	-	18	76 (152)	25

Steady state photolysis of a solution of 100 μM Ruβ in 25 mL DMF:H_2O (1 M) with 0.1 M TEA with 470 nm light in a custom photoreactor, yields a 45.38 μM methanol solution after 1 hour, as determined by head-space GC analysis. While this is only 0.4 TON with respect to methanol, it does represent 2.6 TON per Ru catalyst on an electron basis. . The quantum yield of 1.5 x 10^{-4} for methanol which is more than double that of the $[Ru(phen)_3]^{2+}$ - pyridine system discussed in Chapter 2 and is close to the same system with the addition of KCl. The production of formate in this system is far lower though, with only 0.65 mM being produced and 2.2 mM being produce in the $[Ru(phen)_3]^{2+}$-pyridine from Chapter 2. This could be for a couple of reasons, one of which being the low availability of protonated and reduced pyridine, since there is no excess of pyridine, making it so that further reduction of the substrate is preferred. The other reason, which has not been investigated at this time, is that there is most likely photolablization occurring based on the visual color change observed in the photolysis

solution in a similar manner as in the previous discussed in Chapter 2. While the quantum yield is lower than what was expected it may be possible to improve the photolysis using what was learned from the $Ru(phen)_3^{2+}$ system in Chapter 2, adding a potassium ion or ammonium ions to help the overall efficiency of the system.

3.2.5 Mechanistic details of the CO2 Photocatalytic Reduction by Ruα and Ruβ

Spectroelectrochemical data was used identify the reaction pathways associated with the photocatalytic CO_2 reduction by Ruα and Ruβ complexes. Differential reflectance vs potential curves were used to track the formation of Ruα and Ruβ electroreduced species via the absorbance of the protonated reduced species. These curves were done using N_2 (black line) and CO_2 saturated (red line) solutions monitoring 575 nm, Figure 3.10a, for complex Ruα and 564 nm, Figure 3.10b. The data shown for the forward and reverse scan and the vertical scale is such that the appearance of electrochemically generated species gives rise to positive δR/R signals, regardless of the direction of the scan.

Electrochemical reduction of Ruα and Ruβ, in N_2 saturated solutions show sharp peaks on both the forward and reverse scans (Figure 3.10, black traces) reaching a maximum at -0.65 V and at -0.60 V respectively and in agreement with the voltammetric behavior of the complexes (see Figure 3.3a).. Given the earlier pK_a data, it is presumed that electroreduction is accompanied by protonation in this media (1 M H_2O/DMF) to yield HRu$\beta^{\bullet}$ or HRu$\alpha^{\bullet}$. For both complexes, the intensity of the signal during the reverse scan is higher than that of the forward sweep because the concentration of the reduced species is increasing with time at the electrode interface which is expected for a diffusion controlled process.

In a CO_2 saturated solution, (Figure 3.10, red traces), both complexes the peak intensities observed at 575 nm are significantly reduced for both Ruα and Ruβ, with Ruα

having the greater decrease. This decrease in absorbance shows a decrease in the electroreduce species of Ruα^- and Ruβ^- from interaction with the CO_2 present in solution for modulation is even smaller than for Ru$\beta^{\bullet-}$ because of a dimerization reaction is also consuming the radical in addition to the CO_2. The second situation is supported by photochemical data and by the CV runs, where Ruβ reaches a plateau with a higher current than that of Ruα as shown in Figure 3.4. The δR/R plots not only corroborate that Ruβ is energetically more favorable than Ruα, but also that it reaches higher catalytic currents, meaning it has higher efficiency for CO_2 reduction to its various products.

δR/R/potential curves for complex Ruα were measured at 517 nm to further explain differences in the photochemical mechanism in the absence and presence of CO_2 (Figure 3.11). In the absence of CO_2, the species tracked at 517 nm is formed in the same potential range as that at 575 nm (Figure 3.11). However, in the presence of CO_2, the signal at 517 nm practically disappears. The peak at 517 nm is tentatively being assigned to the reduction of Ruα to the formation of a σ bonded dimer which is found in significantly smaller amounts than that of the monomer (red and black traces in Figure 3.10). The dimer signal is significantly attenuated in the presence of CO_2 (blue trace in Figure 3.11) because of the competition between the reaction of the HRuα with CO_2 and the formation of a σ-dimer (*vide infra*). This dimerization reaction does not seems to occur with complex Ruβ as supported by no optical signal at 517 nm in the δR/R-potential trace either in the absence and presence of CO_2.

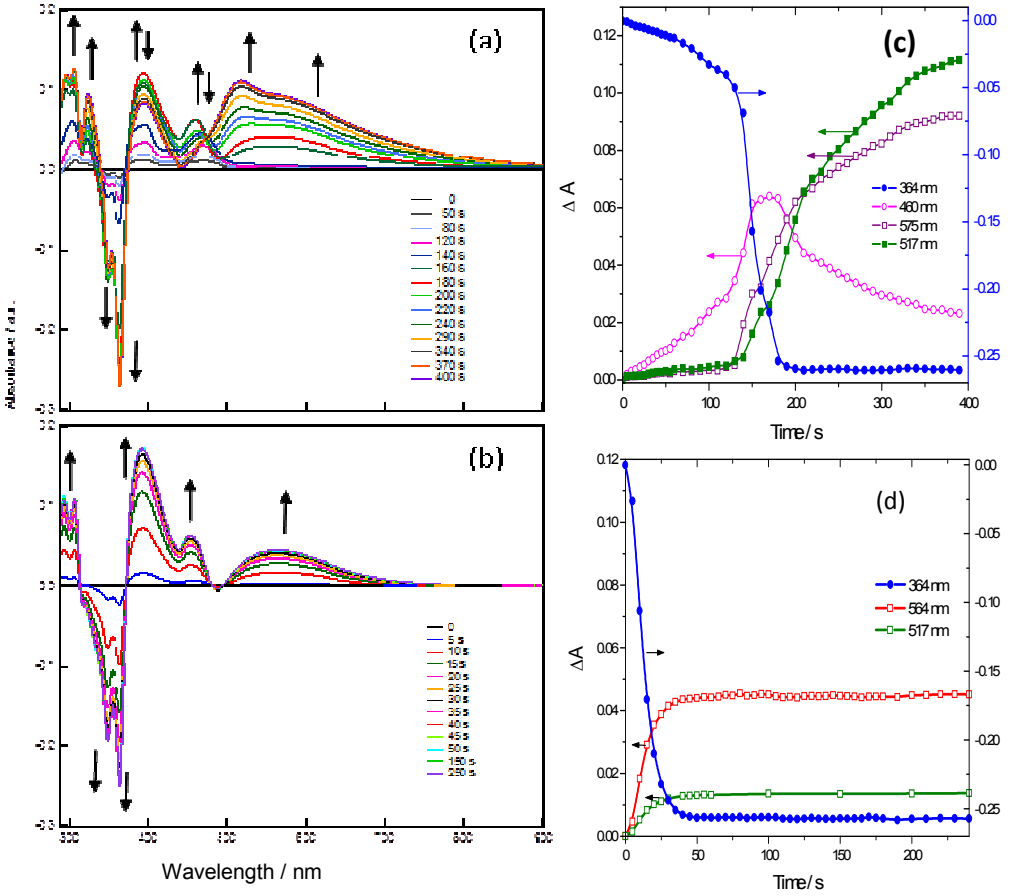

Figure 3.9 Transient ΔA spectra of **Ruα** (2.2 x 10^{-4} M) during photolysis in N_2 saturated (a) and in CO_2 (b) saturated DMF/TEA (0.25 M)/H_2O (1 M) solutions. Peaks pointing down indicate bands disappearing while those pointing up correspond to new bands appearing as a consequence of the photochemical reaction. ΔA were obtained every 5s although only selected spectra are shown in this figure.Photochemical evolution of selected peaks of **Ruα** (2.2 x 10^{-4} M) in the absence (c) and in the presence of CO_2 (d). Data taken from a and b. Total irradiation time was 400 s in N_2 and 250 s in CO_2. Both periods of time were exceeding the attainment of the spectral stationary state.

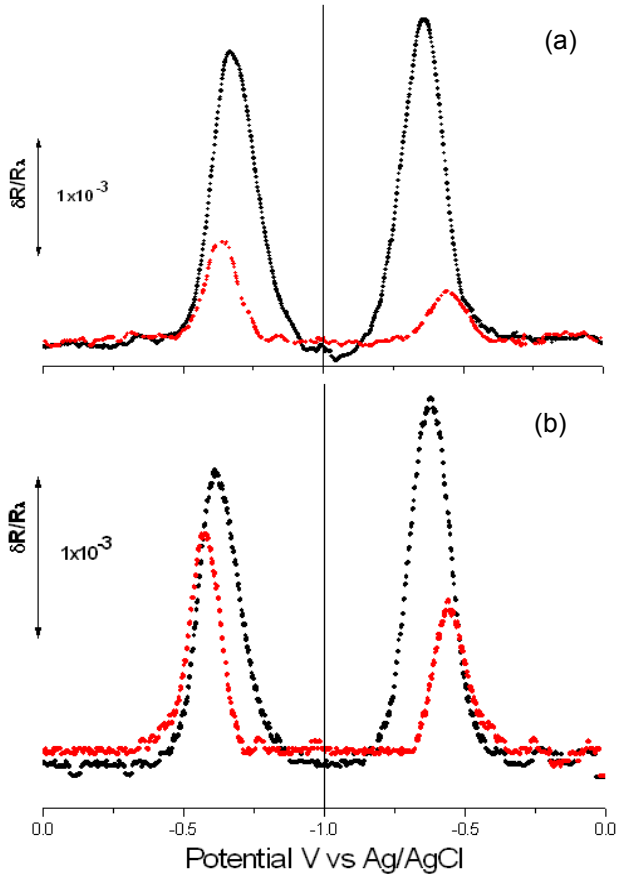

Figure 3.10 δR/R vs. potential curves of **Ruα** at 575 nm (a) and **Ruβ** at 564 nm (b) in DMF containing 0.1 M $TBAPF_6$. These runs were recorded as a function of potentials in Ar (black trace) and CO_2 saturated solutions (red trace). The working electrode was a mirror-polished Pt disc subjected to a sin potential wave (11 Hz, 50 mV_{p-p}) superimposed on a 2 mV/s potential scan.

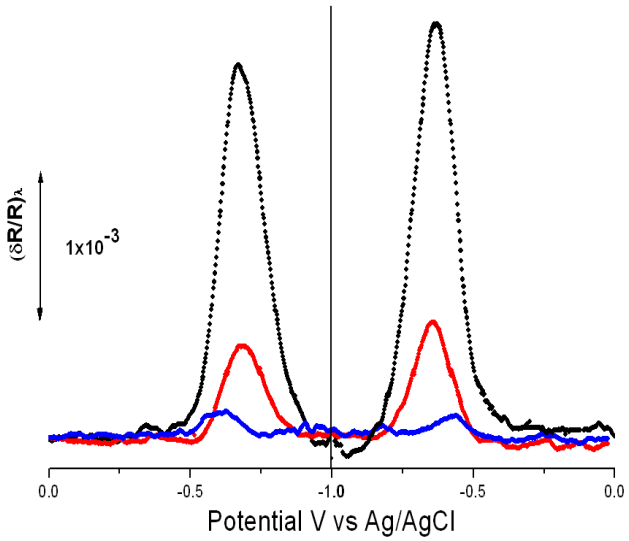

Figure 3.11 Comparison of δR/R vs. potential curves of Ruα at 517 nm in degassed (red) and in CO_2 saturated (blue) DMF containing 0.1 M $TBAPF_6$. For comparison, the trace at 575 (black) in degassed solution is included. Other conditions are as in Figure 3.10.

This differences between Ruα and Ruβ in the δR/R plot in Figure 3.10, show that the amount of radical intermediate is consumed to a greater degree for Ruα than it is for Ruβ in CO_2 saturated solutions. Two possibilities that may give rise to this situation: i) CO_2 reacts faster with radical of Ruα than the radical of Ruβ and therefore is in lower concentrations at the interface and/or ii) in the case of $Ru\alpha^{\bullet-}$ the concentration available The following catalytic mechanism for the first photochemical and electrochemical reduction of Ruα is proposed as follows:

$$Ru\alpha + e^- \rightarrow Ru\alpha^{\bullet-} \quad \text{(the } Ru\alpha^{\bullet-} \text{ is detected at 460 nm)} \quad (1)$$

$$Ru\alpha^{\bullet-} + H_3O^+ \rightarrow HRu\alpha + H_2O \quad \text{(HRuβ detected at 575 nm)} \quad (2)$$

$$Ru\alpha^{\bullet-} + Ru\alpha \rightarrow \sigma\text{-dimer} \quad (\sigma\text{-dimer detected at 517 nm}) \quad (3)$$

$$6\ HRu\alpha + CO_2 \rightarrow 6\ Ru\alpha + CH_3OH + H_2O \quad (4)$$

For complex Ruβ, the reduction does not involve σ-dimer formation, and therefore a typical photocatalytic mechanism is proposed as follows:

$$Ru\beta + e^- \rightarrow Ru\beta^{\bullet-} \quad (Ru\beta^{\bullet-} \text{ detected at 460 nm}) \quad (5)$$

$$Ru\beta^{\bullet-} + H_3O^+ \rightarrow HRu\beta + H_2O \quad (HRu\beta \text{ detected at 564 nm}) \quad (6)$$

$$6\ HRu\beta + CO_2 \rightarrow 6\ Ru\beta + CH_3OH + H_2O \quad (7)$$

As reactions (5) and (7) proceed, the DMF:H_2O mixed solvent is undergoing proton depletion leading to a decrease in the rate of methanol production. This assertion is supported by constant-current electrolysis data, Figure 3.5, during which the potential of the first electroreduction peak was shown to generate methanol and other minor intermediates, such formaldehyde. However, as the electrolysis time progresses the potential evolves toward the second electroreduction process which is mainly the conversion of CO_2 to CO. From the electrochemical and photochemical data it can be

extracted that Ruβ is a better catalyst for CO_2 reduction than Ruα because: i) it lacks the dimerization side reaction which decreases the efficiency of the CO_2 reduction process, and ii) it functions at slightly more positive reduction potentials.

3.3 Conclusions

Both complexes Ruα and Ruβ are competent for photodriven CO_2 reduction in DMF solutions. Both of them show fast, facile, and reversible one-electron reduction and protonation by electrochemical and photochemical methods. Electrocatalytic reduction of CO_2 occurs at the potential of the first electroreduction process for each respective complex (-0.57 V for Ruβ and -0.64 V for Ruα) but the reduction process in Ruα is complicated by a radical-dimerization side reaction which is fast in absence of CO_2.

Identification of all of the photochemically relevant redox and protonated states of the two complexes were obtained by a combination of voltammetry and differential reflectance measurements. Spectroelectrochemistry was particularly useful to probe the photochemical and electrochemical reduction mechanism of both complexes as well as the complexes speciation in the absence and presence of CO_2. Ruβ was found to be a better photo- and electrocatalyst for CO_2 reduction than Ruα due to dimerization reaction that deactivates the complex to CO_2 reducction. Chromatographic analyses of products generated at constant-current electrolyses and constant photolysis revealed the formation of methanol as the main CO_2 reduction product.

3.4 Experimental

3.4.1 Synthesis

$RuCl_3$•3 H_2O was purchased from Pressure Chemical and used as received. DMF, ethanol and acetone were purchased from VWR and used as received. Ammonium Hexafluorophosphate and 1,10-phenanthroline were purchased from Alpha Aesar and used as received, 3,4-diaminopyridine, 2,3-diaminopyridine and

phenylenediamine were purchased from Sigma Aldrich and used as received. $[(phen)_2Ru(pbtp_\beta)](PF_6)_2$, $[(phen)_2Ru(pbtp_\alpha)](PF_6)_2$, $[(phen)_2Ru(dppz)](PF_6)_2$ were synthesized according to standard proceedures.[176,179]

3.4.2 Electrochemistry and Spectroelectrochemistry

Electrochemical data were obtained on a CHI 620C electrochemical analyzer (CH Instruments, Austin, TX, USA) using a single compartment (3-mL volume) electrochemical cell. A glassy carbon (1.5 mm diameter disk) working electrode from Cypress Systems was used. The electrode was polished to a mirror finish with wet alumina (Buehler, 0.05 μm), followed by rinsing with Millipore Milli-Q water and sonication. A platinum wire and a Ag/AgCl reference electrode (Cypress, model EE009) were used as counter and reference electrodes respectively. The electrolyte solutions contains the ruthenium complex in DMF:H_2O(1 M) containing 0.1 M tetrabutylammonium hexafluorophosphate ($TBAPF_6$) as the supporting electrolyte. The solutions were degased or degased and saturated with CO_2 prior to each measurement and the atmosphere was maintained over the electrochemical solution throughout the course of the experiment. All experiments were performed at laboratory ambient temperature (20 ± 2 °C).

Spectroelectrochemistry experiments were performed on platinum disk polished to a mirror finish and used as the working electrode. A platinum coil was used as a counterelectrode and was placed in a separate compartment with a fritted end. The reference electrode was a Ag/AgCl, satd. KCl, and was used with a Luggin capillary to minimize uncompensated ohmic resistance in the cell. Oxygen was exhaustively removed from the working electrode compartment by bubbling N_2 or CO_2 depending on the particular experiment.

Differential reflectivity in the form of δR/R vs potential profiles were recorded on a 2 mV/s potential scan with a superimposed, small amplitude sinusoidal, potential perturbation (ca. 50 mVp-p, 11 Hz). Monochromatic light of a desired wavelength was reflected off the working electrode, a mirror-polished platinum foil, and focused on a photomultiplier operating at a constant current set by a feedback system and a programmable power supply. AC voltammetry was used in some cases along with δR/R measurements. The rectified AC current and optical AC response (normally the in-phase component) were monitored, after demodulation with a lock-in amplifier, as a function of the electrode potential.[180-182]

3.4.3 Photochemical Reduction

All solutions were run in a glass Schlenk cuvette which was degased with N_2 or with CO_2 gas prior to irradiation. Triethylamine (TEA) was present at 0.25 M concentration to serve as a sacrificial donor. The cuvette was placed in a photoreactor with point source lights emitting at 470 nm ± 20 nm. The photon flux was 1×10^{-5} photons/second as measured by chemical actinometry using potassium ferrioxalate.(ref) The progress of the photochemical reaction of Ruα (2.2×10^{-4} M), Ruβ (2.2×10^{-4} M) and Rudppz (1.1×10^{-4} M), was monitored by recording the respective electronic spectra at selected irradiation intervals.

Bulk photolysis solutions were done using 99 μM of the desired complex in 25 mL DMF:water (1 M) and 0.1 M TEA. The solution was irradiated with 470 nm ± 20 nm, from the photoreactor mentioned above, while the solution was kept at 25 °C with a slight positive CO_2 pressure. Aliquots of 5 mL were placed in 4 dram vials and kept at -20 °C until analyzed using head space analysis described below.

3.4.4 Constant-Current Electrolyses

A two-compartment cell with a large area reticulated vitreous carbon (RCV) cylindrical working electrode (BASI # MF-2077) contacted with a platinum wire was placed in the cell's main compartment along with the reference electrode. Platinum foil (2 cm x 8 cm) was used as the counter electrode and was placed within an inner compartment separated by a glass fritt from the main compartment. The working electrode compartment contained 300 μM of the respective ruthenium complex in DMF:H_2O (1 M) solution with 0.1 M $TBAPF_6$ as supporting electrolyte. The counter electrode compartment contained the supporting electrolyte solution but no ruthenium complex. The cell was saturated with CO_2 and kept pressurized and sealed while the electrolyses were performed at an applied current of -0.6 mA.

3.4.5 Product Detection

Gas chromatography (GC) and colorimetric tests were adopted to analyze the conversion of CO_2 to organic products. A Shimadzu GC with mass spectrometer detector (GC-MS-2010 Plus chromatograph with a MS TQ8030 detector) with a AOC-5000 Plus autosampler was used. The chromatographic column (SHRX105MS, 30-m length and 0.25-mm inner diameter) with an oven temperature of 45 °C and the MS source temperature of 250 °C, with helium as carrier gas were used. Detection at m/z = 28, 29 and 31 was chosen to detect methanol, formaldehyde and carbon monoxide as the electrolysis products. Liquid aliquots, periodically withdrawn from the electrochemical cell, were preheated at 80 °C in a 20 mL headspace vial with a septa cap and 2.5 mL of the head space gas was injected from a syringe heated to 80 °C and analyzed in the GC-MS instrument. Control samples containing standard concentrations of methanol (in the range 5-1000 μM) were prepared and run to obtain a quantitative analysis.

A semi-quantitative colorimetric procedure (chromotropic test) was used for corroborate the formaldehyde formation.[73,161,183] As this test is primarily for formaldehyde detection, aliquots (0.5 mL) extracted during the electrolysis experiments were pre-treated to reduce any formic acid to formaldehyde using magnesium turnings under acidic conditions.[183]

REFERENCES

(1) Barton-Cole, E.; Lakkaraju, P. S.; Rampulla, D. M.; Morris, A. J.; Abelev, E.; Bocarsly, A. B. *J. Am. Chem. Soc.* **2010**, *132*, 11539-51.
(2) Seshadri, G.; Lin, C.; Bocarsly, A. B. *J. Electroanal. Chem.* **1994**, *372*, 145-50.
(3) Fenton, H. H. *J. Chem. Soc., Transactions* **1907**, *91*, 687-93.
(4) Royer, M. E. *Comptes rendus hebdomadaires des séances de l'Académie des sciences* **1870**, *70*, 731.
(5) (France), A. d. s. *Comptes rendus hebdomadaires des séances de l'Académie des sciences* **1893**, *116*, 1145.
(6) Spinner, N. S.; Vega, J. A.; Mustain, W. E. *Cat. Sci. Tech.* **2012**, *2*.
(7) Kumar, B.; Llorente, M.; Froelich, J.; Dang, T.; Sathrum, A. J.; Kubiak, C. P. *Annu. Rev. Phys. Chem.* **2012**, *63*, 541-69.
(8) Hoffmann, M. R.; Moss, J. A.; Baum, M. M. *Dalton* **2011**, *40*, 5151.
(9) Cole, E. B.; Bocarsly, A. B. *Carbon Dioxide as Chemical Feedstock*; Wiley-VCH: Weinheim, 2011.
(10) Morris, A. J.; Meyer, G. J.; Fujita, E. *Accounts Chem. Res.* **2009**, *42*, 1983.
(11) Benson, E. E.; Kubiak, C. P.; Sathrum, A. J.; Smieja, J. M. *Chem. Soc. Rev.* **2009**, *38*, 89-99.
(12) Reda, T.; Plugge, C. M.; Abram, N. J.; Hirst, J. *Proc. Natl. Acad. Sci.* **2008**, *105*, 10654.
(13) Hori, Y. *Mod Aspects Electrochem.* **2008**, 42, 89-189.
(14) DuBois, D. L. In *Encyclopedia of Electrochemistry*; Bard, A. J., Stratmann, M., Eds.; Wiley-VCH: Weinheim, 2007; Vol. 7a, p 202.
(15) Taniguchi, I. *Mod. Aspects Electrochem.* **1989**, *20*, 327-400.
(16) Collin, J. P.; Sauvage, J. P. *Coord. Chem. Rev.* **1989**, *93*, 245-68.
(17) Doherty, M. D.; Grills, D. C.; Muckerman, J. T.; Polyansky, D. E.; Fujita, E. *Coord. Chem. Rev.* **2010**, *254*, 2472-82.
(18) Morris, A. J.; Meyer, G. J.; Fujita, E. *Accounts Chem. Res.* **2009**, *42*, 1983-94.
(19) Bockris, J. O. M.; Wass, J. C. *J. Electrochem. Soc.* **1989**, *136*, 2521.
(20) Chandrasekharan, K.; Bockris, J. O. M. *Surface Science* **1987**, *185*, 495.
(21) *Solar Hydrogen Generation: Toward a renewable Energy Future*; Rajeshwar, K.; McConnell, R.; Licht, S., Eds.; Kluwer Academic: New York, 2008.
(22) Service, R. F. *Science* **2011**, *334*, 925-7.
(23) Furuya, N.; Matsui, K. *J. Electroanal. Chem.* **1989**, *271*, 181 - 91.
(24) Gennaro, A.; Isse, A. A.; Vianello, E. In *NATO ASI Series*; Pombeiro, A. J. L., McCleverty., J. A., Eds.; KLUWER ACADEMIC PUBLISHERS B.V.: P.O. Box 322, NL-3300 AH Dordrecht, The Netherlands, 1992; Vol. 385, p 311-6.
(25) Isse, A. A.; Gennaro, A.; Vianello, E.; Floriani, C. *J. Mol. Cat.* **1991**, *70*, 197-208.
(26) Pearce, D. J.; Pletcher, D. *J. Electroanal. Chem. Interfacial Electrochem.* **1986**, *197*, 317-30.
(27) Pun, S.-N.; Chung, W.-H.; Lam, K.-M.; Guo, P.; Chan, P.-H.; Wong, K.-Y.; Che, C.-M.; Chen, T.-Y.; Peng, S.-M. *J. Chem. Soc., Dalton* **2002**, 575-83.
(28) Song, W.; Chen, Z.; Brennaman, M. K.; Concepcion, J. J.; Patrocinio, A. O. T.; Iha, N. Y. M.; Meyer, T. J. *Pure Appl. Chem.* **2011**, *83*, 749-68.
(29) Costamagna, J.; Canales, J.; Vargas, J.; Ferraudi, G. *Pure Appl. Chem.* **1995**, *67*, 1045-52.
(30) Sakaki, S. *J. Am. Chem. Soc.* **1992**, *114*, 2055-62.
(31) Beley, M.; Collin, J. P.; Ruppert, R.; Sauvage, J. P. *J. Am. Chem. Soc.* **1986**, *108*, 7461-7.

(32) Beley, M.; Collin, J.-P.; Ruppert, R.; Sauvage, J.-P. *J. Chem. Soc., Chem. Comm.* **1984**, 1315-6.
(33) Rios-Escudero, A.; Isaacs, M.; Villagran, M.; Zagal, J.; Costamagna, J. *Journal of the Argentine Chemical Society* **2004**, *92*, 63-71.
(34) Scibioh, M. A.; Virayaraghavan, V. R. *B. Electochem.* **1997**, *13*, 275-9.
(35) Scihioh, M. A.; Virayaraghavan, V. R. *B. Electochem.* **2000**, *16*, 376-81.
(36) De, A. C.; Crayston, J. A.; Cromie, T.; Eisenblatter, T.; Hay, R. W.; Lampeka, Y. D.; Tsymbal, L. V. *Electrochim. Acta* **2000**, *45*, 2061-74.
(37) Adaev, I. S.; Korostoshevskaya, T. V.; Novikov, V. T.; Lysyak, T. V. *Russ J. Electrochem.* **2005**, *41*, 1125-9.
(38) Atoguchi, T.; Aramata, A.; Kazusaka, A.; Enyo, M. *J. Chem. Soc., Chem. Comm.* **1991**, 156-7.
(39) Behar, D.; Dhanasekaran, T.; Neta, P.; Hosten, C. M.; Ejeh, D.; Hambright, P.; Fujita, E. *J. Phys. Chem. A* **1998**, *102*, 2870-7.
(40) Nielsen, I. M. B.; Leung, K. *J. Phys. Chem. A* **2010**, *114*, 10166-73.
(41) Tezuka, M.; Iwasaki, M. *Chem. Lett.* **1993**, 427-30.
(42) Bhugun, I.; Lexa, D.; Savéant, J.-M. *J. Am. Chem. Soc.* **1994**, *116*, 5015-6.
(43) Bhugun, I.; Lexa, D.; Savéant, J.-M. *J. Phys. Chem.* **1996**, *100*, 19981-5.
(44) Hammouche, M.; Lexa, D.; Momenteau, M.; Saveant, J. M. *J. Am. Chem. Soc.* **1991**, *113*, 8455-66.
(45) Hammouche, M.; Lexa, D.; Savéant, J. M.; Momenteau, M. *J. Electroanal. Chem. Interfacial Electrochem.* **1988**, *249*, 347-51.
(46) Arana, C.; Keshavarz, M.; Potts, K. T.; Abruña, H. D. *Inorg. Chim. Acta* **1994**, *225*, 285-95.
(47) Ramos, S. J. A.; Arana, C. R.; Hernandez, L.; Potts, K. T.; Keshevarz-K, M.; Abruna, H. D. *Inorg. Chem.* **1995**, *34*, 3339-48.
(48) Daniele, S.; Ugo, P.; Bontempelli, G.; Fiorani, M. *J. Electroanal. Chem. Interfacial Electrochem.* **1987**, *219*, 259-71.
(49) Ishida, H.; Tanaka, K.; Tanaka, T. *Chem. Lett.* **1985**, 405-6.
(50) Ishida, H.; Tanaka, K.; Tanaka, T. *Organometallics* **1987**, *6*, 181-6.
(51) Ishida, H.; Fujiki, K.; Ohba, T.; Ohkubo, K.; Tanaka, K.; Terada, T.; Tanaka, T. *J. Chem. Soc., Dalton* **1990**, 2155-60.
(52) Ishida, H.; Tanaka, H.; Tanaka, K.; Tanaka, T. *J. Chem. Soc., Chem. Comm.* **1987**, 131-2.
(53) Tanaka, H.; Nagao, H.; Peng, S. M.; Tanaka, K. *Organometallics* **1992**, *11*, 1450-1.
(54) Bruce, M. R. M.; Megehee, E.; Sullivan, B. P.; Thorp, H.; O'Toole, T. R.; Downard, A.; Meyer, T. J. *Organometallics* **1988**, *7*, 238-40.
(55) Hawecker, J.; Lehn, J. M.; Ziessel, R. *Helv. Chim. Acta* **1986**, *69*, 1990-2012.
(56) Sullivan, B. P.; Bolinger, C. M.; Conrad, D.; Vining, W. J.; Meyer, T. J. *J. Chem. Soc., Chem. Comm.* **1985**, 1414-6.
(57) Breikss, A. I.; Abruna, H. D. *J. Electroanal. Chem.* **1986**, *201*, 347-58.
(58) Hawecker, J.; Lehn, J. M.; Ziessel, R. *J. Chem. Soc., Chem. Comm.* **1983**, 536-8.
(59) Hawecker, J.; Lehn, J.-M.; Ziessel, R. *J. Chem. Soc., Chem. Comm.* **1984**, 328-30.
(60) Smieja, J. M.; Kubiak, C. P. *Inorg. Chem.* **2010**, *49*, 9283-9.
(61) Christensen, P.; Hamnett, A.; Muir, A. V. G.; Timney, J. A. *J. Chem. Soc., Dalton* **1992**, 1455-63.
(62) Cosnier, S.; Deronzier, A.; Moutet, J.-C. *Journal of Electroanal. Chem. Interfacial Electrochem.* **1986**, *207*, 315-21.
(63) Bolinger, C. M.; Sullivan, B. P.; Conrad, D.; Gilbert, J. A.; Story, N.; Meyer, T. J. *J. Chem. Soc., Chem. Comm.* **1985**, 796-7.

(64) Bolinger, C. M.; Story, N.; Sullivan, B. P.; Meyer, T. J. *Inorg. Chem.* **1988**, *27*, 4582-7.
(65) Ratliff, K. S.; Lentz, R. E.; Kubiak, C. P. *Organometallics* **1992**, *11*, 1986-8.
(66) Slater, S.; Wagenknecht, J. H. *J. Am. Chem. Soc.* **1984**, *106*, 5367-8.
(67) Szymaszek, A.; Pruchnik, F. P. *J. Organometallic Chem.* **1989**, *376*, 133-40.
(68) DuBois, D. L.; Miedaner, A. *J. Am. Chem. Soc.* **1987**, *109*, 113-7.
(69) Mostafa, H. A. G. M.; Nagaoka, T.; Ogura, K. *Electrochim. Acta* **1997**, *42*, 2577-85.
(70) Szymaszek, A.; Pruchnik, F. *Rhodium Express* **1994**, *5*, 18-22.
(71) Nakazawa, M.; Mizobe, Y.; Matsumoto, Y.; Uchida, Y.; Tezuka, M.; Hidai, M. *B. Chem. Soc. Jpn.* **1986**, *59*, 809-14.
(72) Tomohiro, T.; Uoto, K.; Okuno, H. *J. Chem. Soc., Chem. Comm.* **1990**, 194-5.
(73) Barton, E. E.; Rampulla, D. M.; Bocarsly, A. B. *J. Am. Chem. Soc.* **2008**, *130*, 6342-4.
(74) Morris, A. J.; McGibbon, R. T.; Bocarsly, A. B. *ChemSusChem* **2011**, *4*, 191-6.
(75) Keith, J. A.; Carter, E. A. *Chem. Sci.* **2013**, *4*, 1490-6.
(76) Ziessel, R. *NATO ASI SERIES, Series C* **1987**, *206*, 113-38.
(77) Scibioh, M. A.; Viswanathan, B. *Photo/electrochemistry & photobiology in environment, energy and fuel* **2002**, 1-46.
(78) Amatore, C.; Nadjo, L.; Saveant, J. M. *Nouv. J. Chim* **1984**, *8*, 565-6.
(79) Christensen, P. A.; Hamnett, A.; Muir, A. V. G. *Journal of Electroanal. Chem. Interfacial Electrochem.* **1988**, *241*, 361-71.
(80) Ishida, H.; Tanaka, K.; Morimoto, M.; Tanaka, T. *Organometallics* **1986**, *5*, 724-30.
(81) Tanaka, K. *Kagaku (Kyoto)* **1989**, *44*, 570-5.
(82) Tanaka, K. *Denki Kagaku Oyobi Kogyo Butsuri Kagaku* **1990**, *58*, 989-96.
(83) Ishida, H.; Terada, T.; Tanaka, K.; Tanaka, T. *Inorg. Chem.* **1990**, *29*, 905-11.
(84) Ishida, H.; Tanaka, K.; Tanaka, T. *Chem. Lett.* **1988**, 339-42.
(85) Bruce, M. R. M.; Megehee, E.; Sullivan, B. P.; Thorp, H. H.; O'Toole, T. R.; Downard, A.; Pugh, J. R.; Meyer, T. J. *Inorg. Chem.* **1992**, *31*, 4864-73.
(86) Pugh, J. R.; Bruce, M. R. M.; Sullivan, B. P.; Meyer, T. J. *Inorg. Chem.* **1991**, *30*, 86-91.
(87) Kutal, C.; Corbin, A. J.; Ferraudi, G. *Organometallics* **1987**, *6*, 553-7.
(88) Hayashi, Y.; Kita, S.; Brunschwig, B. S.; Fujita, E. *J. Am. Chem. Soc.* **2003**, *125*, 11976-87.
(89) Kutal, C.; Weber, M. A.; Ferraudi, G.; Geiger, D. *Organometallics* **1985**, *4*, 2161-6.
(90) Takeda, H.; Ishitani, O. *Coord. Chem. Rev.* **2010**, *254*, 346-54.
(91) Inagaki, A.; Akita, M. *Coord. Chem. Rev.* **2010**, *254*, 1220-39.
(92) Hori, H.; Takano, Y.; Koike, K.; Sasaki, Y. *Inorg. Chem. Commun.* **2003**, *6*, 300-3.
(93) Hawecker, J.; Lehn, J. M.; Ziessel, R. *J. Chem. Soc., Chem. Comm.* **1985**, 56-8.
(94) Takeda, H.; Koike, K.; Inoue, H.; Ishitani, O. *J. Am. Chem. Soc.* **2008**, *130*, 2023-31.
(95) Hori, H.; Johnson, F. P. A.; Koike, K.; Ishitani, O.; Ibusuki, T. *J. Photochem. Photobio., A:* **1996**, *96*, 171-4.
(96) Takeda, H.; Koike, K.; Morimoto, T.; Inumaru, H.; Ishitani, O. In *Adv. Inorg. Chem.* 63, 137-86.
(97) Hori, H.; P. A. Johnson, F.; Koike, K.; Takeuchi, K.; Ibusuki, T.; Ishitani, O. *J. Chem. Soc., Dalton* **1997**, 1019-23.
(98) Gholamkhass, B.; Mametsuka, H.; Koike, K.; Tanabe, T.; Furue, M.; Ishitani, O. *Inorg. Chem.* **2005**, *44*, 2326-36.
(99) Sato, S.; Koike, K.; Inoue, H.; Ishitani, O. *Photochemical & Photobiological Sciences* **2007**, *6*, 454-61.

(100) Bian, Z.-Y.; Sumi, K.; Furue, M.; Sato, S.; Koike, K.; Ishitani, O. *Inorg. Chem.* **2008**, *47*, 10801-3.
(101) Bian, Z.-Y.; Sumi, K.; Furue, M.; Sato, S.; Koike, K.; Ishitani, O. J. Chem. Soc. *Dalton* **2009**, 983-93.
(102) Koike, K.; Naito, S.; Sato, S.; Tamaki, Y.; Ishitani, O. *J. Photochem. Photobio., A* **2009**, *207*, 109-14.
(103) Tamaki, Y.; Watanabe, K.; Koike, K.; Inoue, H.; Morimoto, T.; Ishitani, O. *Faraday Discussions* **2012**, *155*, 115-27.
(104) Fujita, E.; Brunschwig, B. S.; Cabelli, D.; Renner, M. W.; Furenlid, L. R.; Ogata, T.; Wada, Y.; Yanagida, S. *Studies in Surface Science and Catalysis* **1998**, *114*, 97-106.
(105) Craig, C. A.; Spreer, L. O.; Otvos, J. W.; Calvin, M. *J. Phys. Chem.* **1990**, *94*, 7957-60.
(106) Tinnemans, A. H. A.; Koster, T. P. M.; Thewissen, D. H. M. W.; Mackor, A. *Recl. : Trav. Chem. Pay B.* **1984**, *103*, 288-95.
(107) Grant, J. L.; Goswami, K.; Spreer, L. O.; Otvos, J. W.; Calvin, M. *J. Chem. Soc., Dalton* **1987**, 2105-9.
(108) Kimura, E.; Wada, S.; Shionoya, M.; Okazaki, Y. *Inorg. Chem.* **1994**, *33*, 770-8.
(109) Kimura, E.; Bu, X.; Shionoya, M.; Wada, S.; Maruyama, S. *Inorg. Chem.* **1992**, *31*, 4542-6.
(110) Matsuoka, S.; Yamamoto, K.; Ogata, T.; Kusaba, M.; Nakashima, N.; Fujita, E.; Yanagida, S. *J. Am. Chem. Soc.* **1993**, *115*, 601-9.
(111) Ogata, T.; Yamamoto, Y.; Wada, Y.; Murakoshi, K.; Kusaba, M.; Nakashima, N.; Ishida, A.; Takamuku, S.; Yanagida, S. *J. Phys. Chem.* **1995**, *99*, 11916-22.
(112) Ogata, T.; Yanagida, S.; Brunschwig, B. S.; Fujita, E. *J. Am. Chem. Soc.* **1995**, *117*, 6708-16.
(113) Grodkowski, J.; Behar, D.; Neta, P.; Hambright, P. *J. Phys. Chem. A* **1997**, *101*, 248-54.
(114) Amatore, C.; Saveant, J. M. *J. Am. Chem. Soc.* **1981**, *103*, 5021-3.
(115) Olah, G. A.; Prakash, G. K. S.; Goeppert, A. *J. Am. Chem. Soc.* **2011**, *133*, 12881-98.
(116) Goeppert, A.; Czaun, M.; May, R. B.; Prakash, G. K. S.; Olah, G. A.; Narayanan, S. R. *J. Am. Chem. Soc.* **2011**, *133*, 20164-7.
(117) Finn, C.; Schnittger, S.; Yellowlees, L. J.; Love, J. B. *Chem. Commun.* **2012**, *48*, 1392-9.
(118) Cokoja, M.; Bruckmeier, C.; Rieger, B.; Herrman, W. A.; Kuhn, F. E. *Angew. Chem. Int. Ed.* **2011**, *50*, 8510-37.
(119) Cole-Barton, E.; Lakkaraju, P. S.; Rampulla, D. M.; Morris, A. J.; Abelev, E.; Bocarsly, A. B. *J. Am. Chem. Soc.* **2010**, *132*, 11539-51.
(120) Dimitrijevic, N. M.; Vijayan, B. K.; Poluektov, O. G.; Rajh, T.; Gray, K. A.; He, H.; Zapol, P. *J. Am. Chem. Soc.* **2011**, *133*, 3964-71.
(121) Garrison, W. M.; Morrison, D. C.; Hamilton, J. G.; Benson, A. A.; Calvin, M. *Science* **1951**, *114*, 416-8.
(122) Halmann, M. *Nature* **1978**, *275*, 115-6.
(123) Hawecker, J.; Lehn, J.-M.; Ziessel, R. *Helv. Chim. Acta* **1986**, *69*, 1990-2012.
(124) Inoue, T.; Fujishima, A.; Konishi, S.; Honda, K. *Nature* **1979**, *277*, 637-8.
(125) Naitoh, A.; Ohta, K.; Mizuno, T.; Yoshida, H.; Sakai, M.; Noda, H. *Electrochim. Acta* **1993**, *38*, 2177-9.
(126) Sayama, K.; Arakawa, H. *J. Phys. Chem.* **1993**, *97*, 531-3.
(127) O'Toole, T. R.; Meyer, T. J.; Sullivan, B. P. *Chem. Mater.* **1989**, *1*, 574-6.

(128) O'Toole, T. R.; Sullivan, B. P.; Bruce, M. R. M.; Margerum, L. D.; Murray, R. W.; Meyer, T. J. *J. Electroanal. Chem. Interfacial Electrochem.* **1989**, *259*, 217-39.
(129) Chen, Z.; Chen, C.; Weinberg, D. R.; Kang, P.; Concepcion, J. J.; Harrison, D. P.; Brookhart, M. S.; Meyer, T. J. *Chem. Comm.* **2011**, *47*, 12607-9.
(130) Grodkowski, J.; Dhanasekaran, T.; Neta, P.; Hambright, P.; Brunschwig, B. S.; Shinozaki, K.; Fujita, E. *J. Phys. Chem. A* **2000**, *104*, 11332-9.
(131) Chen, J.; Szalda, D. J.; Fujita, E.; Creutz, C. *Inorg. Chem.* **2010**, *49*, 9380-91.
(132) Kelly, C. A.; Mulazzani, Q. G.; Venturi, M.; Blinn, E. L.; Rodgers, M. A. J. *J. Am. Chem. Soc.* **1995**, *117*, 4911-9.
(133) Jacquet, O.; Frogneux, X.; Das Neves Gomes, C.; Cantat, T. *Chem. Sci.* **2013**, *4*, 2127-31.
(134) Costentin, C.; Drouet, S.; Robert, M.; Saveant, J. M. *Science* **2012**, *338*, 90-4.
(135) Costentin, C.; Robert, M.; Saveant, J. M. *Chem. Soc. Rev.* **2013**, *42*, 2423-36.
(136) Das Neves Gomes, C.; Jacquet, O.; Villiers, C.; Thuery, P.; Ephritikhine, M.; Cantat, T. *Angew. Chem. Int. Ed.* **2012**, *51*, 187-90.
(137) Jeoung, J.-H.; Dobbek, H. *Science* **2007**, *318*, 1461-4.
(138) Hori, H.; Ishihara, J.; Koike, K.; Takeuchi, K.; Ibusuki, T.; Ishitani, O. *J. Photochem. Photo. A:* **1999**, *120*, 119-24.
(139) Savéant, J.-M. *Chem. Rev.* **2008**, *108*, 2348-78.
(140) Olah, G. A.; Goeppert, A.; Prakash, G. K. S. *J. Org. Chem.* **2009**, *74*, 487-98.
(141) Keith, J. A.; Carter, E. A. *J. Am. Chem. Soc.* **2012**, *134*, 7580-3.
(142) Yasukouchi, K.; Taniguchi, I.; Yamaguchi, H.; Shiraishi, M. *J. Electroanal. Chem. and Interfacial Electrochem.* **1979**, *105*, 403-8.
(143) MacDonnell, F. M. In *Solar Hydrogen Generation: Toward a renewable energy future*; Rajeshwar, K., McConnell, R., Licht, S., Eds.; Springer Science+Business Media, LLC: New York, New York, 2008.
(144) Bolletta, F.; Moggi, L.; Hug, G. *J. Phys. Chem. Ref. Data.* **1988**, *18*, 219-543.
(145) Tinnemans, A. H. A.; Koster, T. P.; Thewissen, D. H. M. W.; Mackor, A. *Recl. Trav. Chim. Pays-Bas* **1984**, *103*, 288-95.
(146) Krishnan, C. V.; Sutin, N. *J. Am. Chem. Soc.* **1981**, *103*, 2141-2.
(147) Darensbourg, D. J.; Pala, M. *J. Am. Chem. Soc.* **1985**, *107*, 5687-93.
(148) Willner, I.; Maidan, R.; Mandler, D.; Duerr, H.; Doerr, G.; Zengerle, K. *J. Am. Chem. Soc.* **1987**, *109*, 6080-6.
(149) Fujita, E. *Coord. Chem. Rev.* **1999**, *185-186*, 337-84.
(150) Durham, B.; Caspar, J. V.; Nagle, J. K.; Meyer, T. J. *J. Am. Chem. Soc.* **1982**, *104*, 4803-10.
(151) Ertem, M. Z.; Konezny, S. J.; Araujo, C. M.; Batista, V. S. *J. Phys. Chem. Lett.* **2013**, *4*, 745-8.
(152) Lim, C.-H.; Holder, A. M.; Musgrave, C. B. *J. Am. Chem. Soc.* **2012**, *135*, 142-54.
(153) Ischay, M. A.; Lu, Z.; Yoon, T. P. *J. Am. Chem. Soc.* **2010**, *132*, 8572-4.
(154) Kuhn, H. J.; Braslavsky, S. E.; Schmidt, R. *Pure Appl. Chem* **2004**, *76*, 2105-46.
(155) Darensbourg, D. J.; Rokicki, A.; Darensbourg, M. Y. *J. Am. Chem. Soc.* **1981**, *103*, 3223-4.
(156) Savéant, J.-M. *Chem. Rev.* **2008**, *108*, 2348-78.
(157) Chen, Z.; Concepcion, J. J.; Brennaman, M. K.; Kang, P.; Norris, M. R.; Hoertz, P. G.; Meyer, T. J. *Proc. Natl. Acad. Sci. U.S.A.* **2012**, *109*.
(158) Fukushima, T.; Fujita, E.; Muckerman, J. T.; Polyansky, D. E.; Tanaka, K.; American Chemical Society: 2009, p PHYS-012.
(159) Grodkowsik, J.; Dhanasekaran, T.; Neta, P.; Hambright, P.; Brunschwig, B. S.; Shinozaki, K.; Fuita, E. *J. Phys. Chem. A* **2000**, *104*, 11332-9.

(160) Haines, R. J.; Wittrig, R. E.; Kubiak, C. P. *Inorg. Chem.* **1994**, *33*, 4723-8.
(161) Arana, C.; Yan, S.; Keshavarz-K, M.; Potts, K. T.; Abruna, H. D. *Inorg. Chem.* **1992**, *31*, 3680-2.
(162) Chiericato, G.; Arana, C.; Casado, C.; Cuadrado, I.; Abruna, H. D. *Inorg. Chimi. Acta* **2000**, *300-302*, 32-42.
(163) Hurrell, H. C.; Mogstad, A. L.; Usifer, D. A.; Potts, K. T.; Abruna, H. D. *Inorg. Chem.* **1989**, *28*, 1080-4.
(164) Crabtree, R. H. In *Carbon Dioxide as Chemical Feedstock*; Aresta, M., Ed.; John Wiley & Sons Ltd.: Weinheim, 2010, p 301-6.
(165) Boston, D. J.; Huang, K.-L.; de Tacconi, N. R.; Myung, N; MacDonnell, F. M.; Rajeshwar, K. In *Photoelectrochemical Water Splitting: Challenges and New Perspectives*; Lewerenz, H. J., Peter, L., Eds.; RSC Press: In Press.
(166) Boston, D. J.; Xu, C.; Armstrong, D. W.; MacDonnell, F. M. *J. Am. Chem. Soc.*, 135, 16252-5.
(167) Jenkins, Y.; Friedman, A. E.; Turro, N. J.; Barton, J. K. *Biochem.* **1992**, *31*, 10809-16.
(168) Nair, R. B.; Cullum, B. M.; Murphy, C. J. *Inorg. Chem.* **1997**, *36*, 962-5.
(169) Montalti, M.; Credi, A.; Prodi, L.; Gandolfi, M. T. *Handbook of Photochemistry*; 3 ed.
(170) Friedman, A. E.; Chambron, J. C.; Sauvage, J. P.; Turro, N. J.; Barton, J. K. *J. Am. Chem. Soc.* **1992**, *112*, 4960-2.
(171) Brennaman, M. K.; Alstrum-Acevedo, J. H.; Fleming, C. N.; Jang, P.; Meyer, T. J.; Papanikolas, J. M. *J. Am. Chem. Soc.* **2002**, *124*, 15094-8.
(172) Sun, Y.; Lutterman, D. A.; Turro, C. *Inorg. Chem.* **2008**, *47*, 6427-3434.
(173) Sun, Y.; Collins, S. N.; Joyce, L. E.; Turro, C. *Inorg. Chem.* **2010**, *49*, 4257-62.
(174) Chen, X.; Gao, F.; Yang, W.-Y.; Sun, J.; Zhou, Z.-X.; Ji, L.-N. *Inorg. Chim. Acta.* **2011**, *378*, 140-7.
(175) Sun, Y.; Turro, C. *Inorg. Chem.* **2010**, *49*, 5025-32.
(176) Tan, L.; Xiao, Y.; Liu, X.; Zhang, S. *Spectrochim. Acta Part A* **2009**, *73*, 858-64.
(177) Fees, J.; Kaim, W.; Mosherosh, M.; Matheis, W.; Klima, J.; Krejcik, M.; Zalis, S. *Inorg. Chem.* **1993**, *32*, 166-74.
(178) Flynn, C. P. *Point Defects ad Diffusion*; Clarendon Press: Oxford, 1972.
(179) Hartshorn, R. M.; Barton, J. K. *J. Am. Chem. Soc.* **1992**, *114*, 5919-25.
(180) Singh, S.; de Tacconi, N. R.; Diaz, N. R. G.; Lezna, R. O.; Muñoz Zuñiga, J.; Abayan, K.; MacDonnell, F. M. *Inorg. Chem.* **2011**, *50*, 9318-28.
(181) de Tacconi, N. R.; Lezna, R. O.; Chitakunye, R.; MacDonnell, F. M. *Inorg. Chem.* **2008**, *47*, 8847-58.
(182) Wolcan, E.; Feliz, M. R.; Ruiz, G. T.; Juliarena, M. P.; Lezna, R. O. *J. Electroanal. Chem. Interfacial Electrochem.* **2002**, *533*, 101-6.
(183) Grant, W. M. *Anal. Chem.* **1948**, *20*, 267-9.

BIOGRAPHICAL INFORMATION

David J. Boston received his Bachelors of Science from Iowa State University in 2006. During his time at Iowa State University he worked under Dr. Aaron Sadow, with whom he studies asymmetric hydrogen transfer from glycerol to acetone using a ruthenium based catalyst. In 2007, David started at the University of Texas at Arlington, where he worked under Dr. Frederick MacDonnell. During the time at the University of Texas at Arlington David work on solar energy projects and focused on the solar reduction of carbon dioxide to methanol.